

Thesis for Master's Degree

# Ultrasound Imaging Super Resolution via Compressive Sensing

Mohamed Yaseen Jabarulla

School of Information and Communications  
Gwangju Institute of Science and Technology

2016

# Ultrasound Imaging Super Resolution via Compressive Sensing

Advisor: Heung-No Lee

by

Mohamed Yaseen Jabarulla

School of Information and Communications

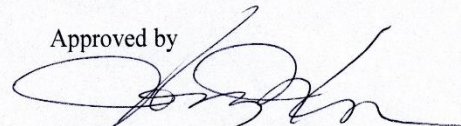
Gwangju Institute of Science and Technology

A thesis submitted to the faculty of the Gwangju Institute of Science and Technology in partial fulfillment of the requirements for the Degree of Master of Science in the School of Information and Communications

Gwangju, Republic of Korea

2015.12.03

Approved by



Professor Heung-No Lee


Committee Chair

# Ultrasound Imaging Super Resolution via Compressive Sensing

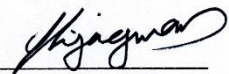
Mohamed Yaseen Jabarulla

Accepted in partial fulfillment of the requirement for the  
Degree of Master of Science

Committee Chair

  
Prof. Heung-No Lee

Committee Member

  
Prof. Jae Gwan Kim

Committee Member

  
Prof. Hyuk Lim

## **Acknowledgments**

I would like to give my sincerest gratitude to my adviser Prof. Heung No-Lee for his patience, guidance, and mentor-ship throughout my thesis. It means a lot to me to have someone looking out for me and providing this opportunity to work under his supervision. I give special thanks to him for introducing this field of research and helping me become a researcher, and for all his support in making better at it.

Special thanks to my family and friends who love me and support me always.

MS/SIC Mohamed Yaseen Jabarulla. Ultrasound imaging super resolution via compressive  
20141001 sensing and its applications.

School of Information and Communications.2016.44P.Prof.Heung-No Lee

## **Abstract**

The recently introduced compressive sensing (CS) theory allows under certain assumptions to recover a signal sampled below the Nyquist sampling limit. Compressive sensing can be applied for two purposes. First, to decrease the number of samples needed to capture the information, thus allowing faster acquisitions. Second, to improve the reconstruction of images in fields where constraints on the physical acquisition setup yield very sparse data sets. This thesis focuses on medical ultrasound, with the following applications: The appearance of granular ‘noise’ referred to as speckle that inherently exists in ultrasound (US) imagery, which decreases the resolutions of US image. Here by using the fact that the image is highly compressible in the wavelet domain and leverage new results of compressed sensing (CS) theory to make an accurate estimate of the original high-resolution of US image. Unfortunately, direct use of a wavelet compression basis not applicable in traditional CS approaches because of the coherency between the point-samples from the subsampling process and the wavelet basis. To overcome this problem, we include the subsampling low-pass filter into our measurement matrix, which decreases coherency between the basis. To invert the subsampling process, we use the appropriate reconstructing algorithm such as greedy, matching pursuit algorithm and obtain the high-resolution US image. The result is a simple and efficient algorithm that can generate high-resolution, high quality US images without the use of data sets. The experimental results show the proposed method is very effective and can get better reconstruction performances.

© 2016

Mohamed Yaseen Jabarulla

ALL RIGHTS RESERVED

**-ii-**

# Contents

<b>Abstract</b> .....	<b>i</b>
<b>Contents</b> .....	<b>iii</b>
<b>List of Figures</b> .....	<b>v</b>
<b>List of Tables</b> .....	<b>vi</b>
<b>1 Introduction</b> .....	<b>1</b>
1.1 Background.....	1
1.2 Motivation.....	1
1.3 Thesis Outline.....	2
<b>2 Ultrasonography</b> .....	<b>2</b>
2.1 Sonographic equipment.....	2
2.1.1 Probe.....	2
2.1.2 Beamforming.....	3
2.1.3 Image quality.....	6
2.2 Interaction between tissues and ultrasound waves.....	7
2.2.1 Wave propagation in an inhomogeneous medium.....	7
2.2.2 Ultrasounds in the body.....	9
2.3 Reconstructing the ultrasound signal.....	10
2.4 Modes of sonography.....	12
2.4.1 M-mode.....	12
2.4.2 B-mode.....	13
2.4.3 Doppler mode.....	14
<b>3 Super Resolution</b> .....	<b>16</b>
3.1 Theory and Background.....	17
3.2 Early super-resolution methods.....	18

3.2.1	Super resolution in frequency domain.....	18
3.2.2	Spatial domain methods.....	19
3.2.3	Projection and interpolation.....	19
3.2.4	Probabilistic methods.....	19
3.2.5	Iterative method.....	20
3.2.6	Projection on to convex sets.....	20
3.2.7	Edge-preservation method.....	21
3.3	Challenges.....	21
<b>4</b>	<b>Compressive sensing.....</b>	<b>23</b>
4.1	Compressive sensing theory.....	23
4.1.1	Background.....	23
4.1.2	The sparsity of signals.....	24
4.1.3	The inefficiencies of conventional data transform.....	24
4.1.4	Motivation.....	25
4.1.5	The introduction of compressed sensing.....	27
4.2	Conditions for successful CS signal recovery .....	28
4.2.1	Restricted isometry property (RIP).....	28
4.2.2	The idea of Reconstruction.....	29
<b>5</b>	<b>Implementation.....</b>	<b>31</b>
5.1	Super Resolution Ultrasound Compressed sensing.....	34
5.2	Experiments on Ultrasound Images.....	36
5.3	Conclusion.....	40
	<b>References.....</b>	<b>41</b>



## List of Figures

Figure 1 (a) Linear array transducer (b) Curved array transducer (c) Phased array transducer.....	3
Figure 2 Principle of beamforming. The principle is the same in emission and reception.....	4
Figure 3 Point spread function phantom imaged without apodization.....	5
Figure 4 Point spread function phantom imaged with apodization.....	5
Figure 5 Electronic focusing and steering of an ultrasound beam.....	6
Figure 6 RF signal processing.....	11
Figure 7 M-mode and B-mode images.....	13
Figure 8 RF sampling of single pulse moving away from the transducer.....	14
Figure 9 The creation of low-resolution image pixels.....	16
Figure 10 One high-resolution image generates a set of low-resolution images.....	17
Figure 11 Aliasing relationship between LR and HR image.....	18
Figure 12 Three of the challenges facing a multi-frame super-resolution algorithm.....	22
Figure 13 An example the Fourier transform of a bandlimited signal $x(t)$ .....	23
Figure 14 Comparison of a random image.....	25
Figure 15 (a) Original Image (b) Reconstructed image (c) Sorted wavelet coefficients of the original image. (d) Sorted wavelet coefficients of the reconstructed image.....	27
Figure 16 A Pictorial representation of CS process.....	28
Figure 17 Comparison of PSNR for different reconstruction algorithm.....	37
Figure 18(a-d): Reconstruction comparison of US images.....	38
Figure 19 Reconstruction error comparison as a function of magnification level for the US phantom image.....	39

## **List of Tables**

Table 1: Approximate densities, sound speeds, characteristic acoustic impedances and attenuation of human tissues.....	9
Table 2: Reflection coefficients in the case of normal incidence.....	10
Table 3: The numerical guidelines of the recovered images obtained from different methods.....	40

# Chapter 1

## Introduction

### 1.1 Background

The recently introduced compressed sensing (CS) theory allows – under certain assumptions to recover a signal sampled below the Nyquist sampling limit [1, 2, 3]. Compressed sensing (also known as compressive sensing or compressive sampling) can be applied for two main purposes:

- It can lower the amount of data needed and thus allows to speed up acquisition. A typical example of such application is dynamic MRI [4].
- It can improve the reconstruction of signals/image in fields where constraints on the physical acquisition setup yield very sparse data sets. A typical example is seismic data recovery in geophysics [5].

### 1.2 Motivation

This thesis focuses on medical ultrasound, In our work, we consider the problem of US Single image super resolution(SISR) and utilizes a novel algorithm for reconstructing the noiseless high resolution image based on the CS [1] [3]. CS brings the possibility of reconstructing a sparse image with fewer measurements than Nyquist sampling theory requires. The key idea is to obtain high resolution US image that will be sparse in a transform domain (e.g., wavelet) and using compressed sensing theory to solve the sparse coefficients from the low-resolution image. Furthermore, recovering an approximation of high-resolution image from the wavelet transform, we can compute the final result in the spatial domain.

## 1.3 Thesis Outline

The thesis is organized as follows: chapter 2 is an introduction to medical ultrasonography. Chapter 3 describes about super resolution. Chapter 4 presents the compressive sensing theory and the algorithms we use for CS signal recovery. Finally, Chapter 5 presents how the CS theory can be applied to ultrasound signal recovery in B-mode imaging and compares the performance obtained with different algorithms.

# Chapter 2

## Ultrasonography

Sonography is a widespread medical imaging method whose principle is based on the propagation of ultrasonic waves in biological tissues. It allows real-time visualization of body structures by displaying their acoustic properties. Ultrasonography has the advantage of being non-invasive, non-ionizing, and relatively cheap compared to other imaging methods such as X ray imaging.

In practice, a probe emits an ultrasonic wave, which is then diffused, reflected and attenuated by different tissue structures. Part of the wave travels back in the direction of the probe, which performs its acquisition and conversion to an electrical signal.

### 2.1 Sonographic equipment

#### 2.1.1 Probe

The ultrasound probe consists of a transducer comprising one or more piezoelectric elements, which can generate an ultrasound wave when excited by an electrical signal. With the ability of piezoelectric materials to convert electrical energy into acoustic energy and vice versa, the transducer are used for both transmission and reception of ultrasonic waves. Depending on the probe type, the ultrasound beam sweeps a rectangular or sectorial area (figure 1). Linear array transducers emits parallel beams and are used e.g. for thyroid and breast cancer detection. Convex probes cover a sectorial zone, which allows to scan deeper and wider structures. Phased array

transducers are also sector probes, but the beam steering is done electronically. These transducers are thus much more compact, which is very useful to avoid obstacles such as ribs in echocardiography. The drawback is that the beam steering requires more complex electronics and creates secondary lobes.

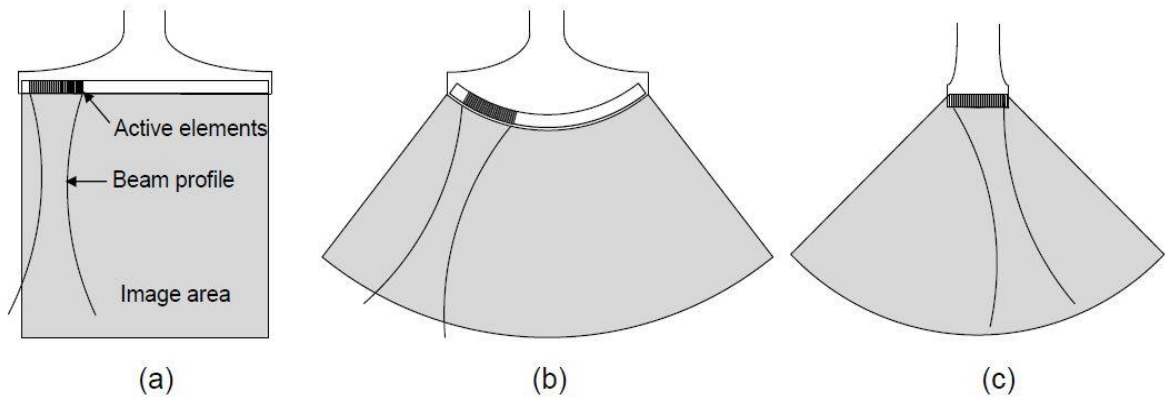


Figure 1: (a) Linear array transducer (b) Curved array transducer (c) Phased array transducer.

## 2.1.2 Beamforming

For better image resolution, the beam is formed by delaying the emission of each element so as to focus the emitted energy on the depth of interest. The principle is the same during reception: before being summed, the signals received by each element can be delayed to allow focusing. The time needed by an echo to travel back to the probe is roughly proportional to the depth of its source. Thus, by adjusting the delay of each element according to the echo depth — that is, according to the time elapsed since the pulse emission — it is possible to maintain a continuous focus or several focal zones during reception. In addition, the focusing of the system can be improved by weighting the contribution of each element. This is called apodization. The whole process is referred to as beamforming, and is illustrated in figure 2. Figure 3 and 4 show point spread functions for different set-up of transmit and receive focusing and apodization. The calculation of point spread functions is done by placing a point in front of the transducer and then sweeping the beam over the point. This gives the point spread function of the imaging system. The phantom used to calculate the PSFs shown in figure 3 and 4 consists of a number of point targets placed with a distance of 5mm starting at 15mm from the transducer surface. More information on the set-up can be found in [6].

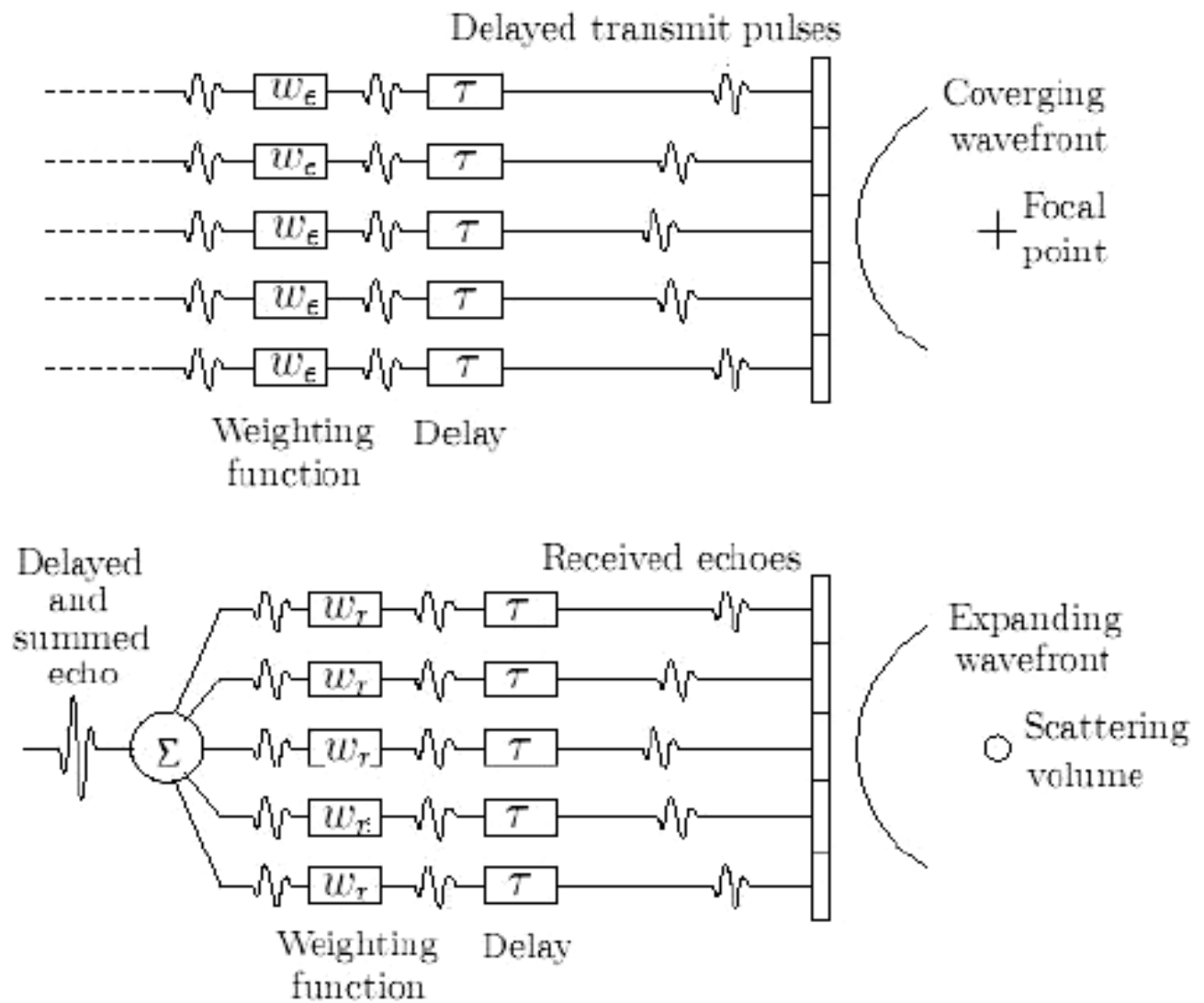


Figure 2: Principle of beamforming. The principle is the same in emission and reception

In the case of phased array transducers, the pulse delaying also allows to steer the beam in the desired direction, as shown in figure 5 [7].

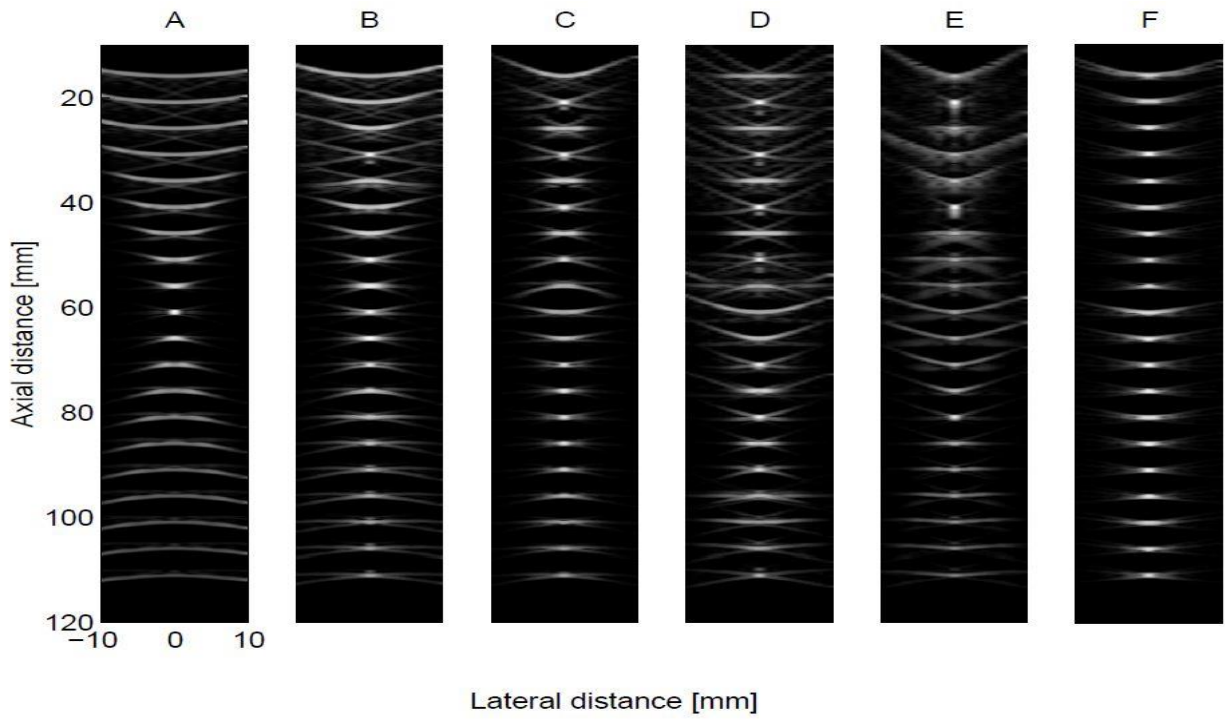


Figure 3: Point spread function phantom imaged without apodization.

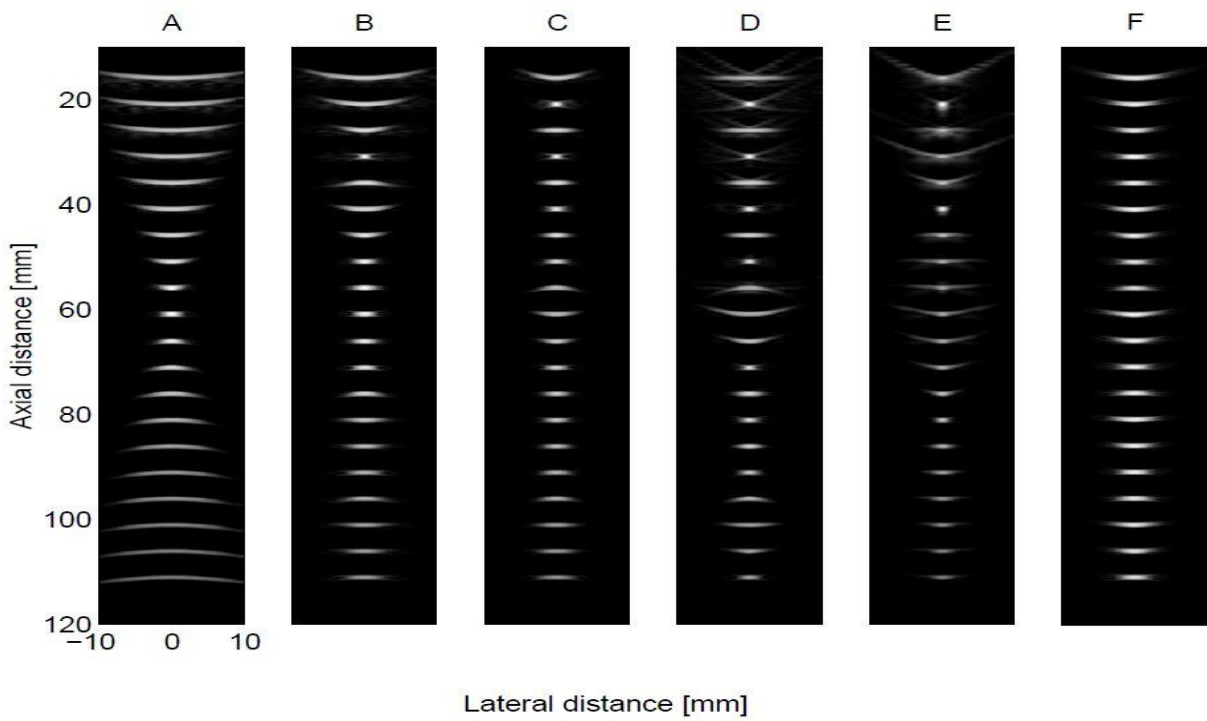


Figure 4: Point spread function phantom imaged with apodization.

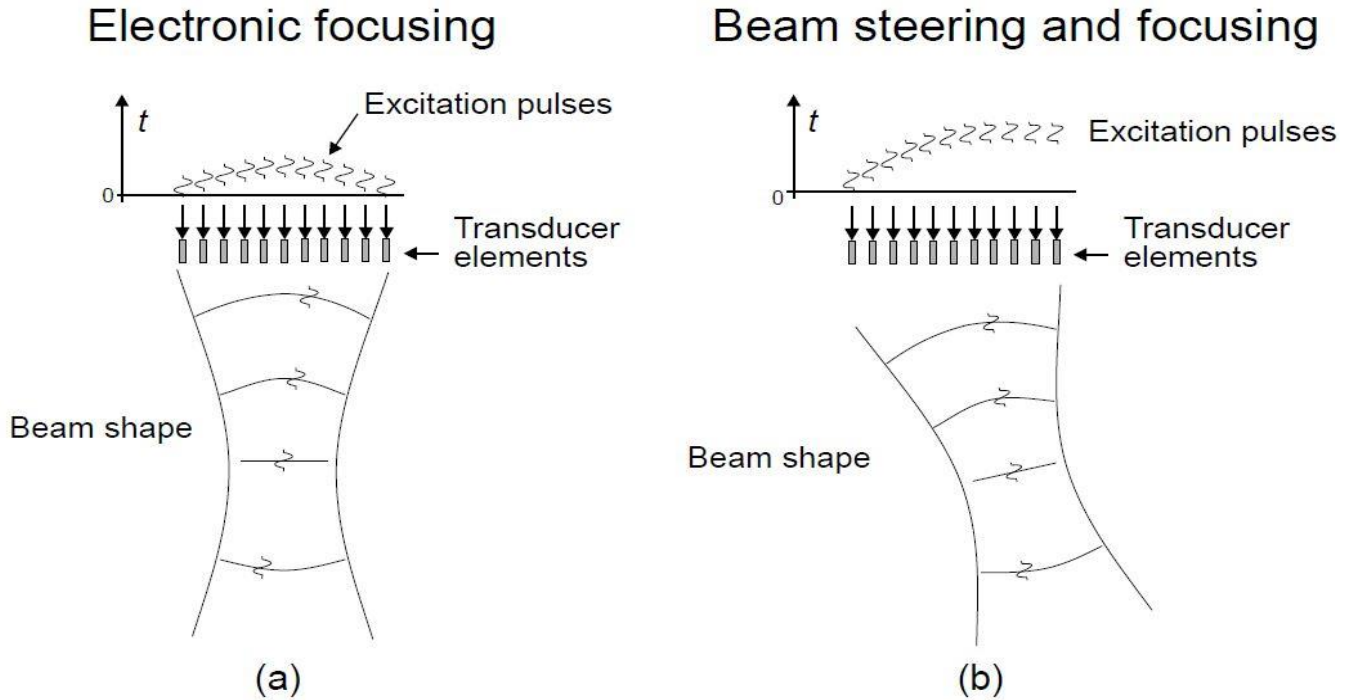


Figure 5: Electronic focusing and steering of an ultrasound beam.

### 2.1.3 Image quality

The quality of an ultrasound image depends strongly on the axial and lateral resolution of the acquisition system.

#### Axial resolution

The axial resolution refers to the resolution in the direction of the propagation, and depends mainly on the frequency of the ultrasound. Higher frequencies correspond to shorter wavelengths and thus give better axial resolution. The frequencies used in ultrasonography usually range from 1 to 20 MHz. However, the attenuation of the sound wave is increased at higher frequencies, so in order to have better penetration of deeper tissues, a lower frequency (3-5 MHz) is used. At 3 Mhz, the axial resolution can be as low as 0.2 mm. More details about attenuation can be found in section 2.2.1.



## Lateral resolution

The lateral resolution of the 2D image depends on the shape of the ultrasound beam, as thinner beams give more laterally resolved images. As explained in section 2.1.2, in modern scanners, the focusing can be adjusted by the operator so that the resolution is optimal in the region of interest.

## 2.2 Interaction between tissues and ultrasound waves

### 2.2.1 Wave propagation in an inhomogeneous medium

In a homogeneous, non-absorbing medium, the direction and amplitude of a plane wave remains constant. This is not the case in biological tissues. Indeed, the wave intensity decreases as it travels deeper into the body, and the wave front does not remain plane. Several factors cause this ultrasound wave attenuation.

#### Diffusion

Diffusion, in the broadest sense, occur when a wave propagates in a non-uniform medium. Part of its energy is redirected and appears separately from the initial wave. For example, this happens when a wave hits a plane interface, thus giving birth to a reflected and refracted wave. However, the plane interface model is valid only when the encountered object is large compared to the wavelength. In the medical domain, such interfaces are uncommon, and discontinuities are very variable in shape, size, position and orientation. Diffusion occur when the dimension of the inhomogeneity is small compared to the wavelength of the incident wave. The inhomogeneity then behaves as a point source emitting the energy in all directions in the form of a spherical wave.

#### Interferences

The ultrasound wave encounters many obstacles that are very close to each other, such as the scatterers described above. Each of them behaves as a point source and emits a spherical wave. These waves are coherent, which causes their superposition to give birth to interferences. This results in the speckle pattern which is typical of ultrasound images. A speckle in an ultrasound image does not correspond to a real object, it only results from constructive interferences.

## Diffraction

When a wave encounters an obstacle whose dimension is close to the wavelength, its propagation direction is deflected by diffraction.

## Absorption

The absorption phenomenon refers to the conversion of the incident ultrasound energy into heat. This can lead to significant loss of energy.

## Attenuation

Attenuation refers to all the losses, that is to say the energy that is not transmitted through the medium and that would not reach a receptor facing the emitting probe. Reflection, refraction, diffusion, diffraction and absorption contribute thus to attenuation. Attenuation is a function of the distance  $z$  traveled by the wave and can be characterized by the coefficient  $\alpha$ , which is generally given in  $dB.cm^{-1}$ :

$$\alpha = -\frac{20}{z} \log \frac{P_z}{P_0}$$

This coefficient is proportional to the frequency. As a consequence, attenuation is a major issue at higher frequencies. In biological tissues, attenuation is about  $1 dB.cm^{-1}.MHz^{-1}$ . To illustrate the effect of attenuation, let us consider a 3MHz probe and compare the amplitude of echoes coming from two identical targets located 10 cm apart — that is, 20 cm round-trip. In this setup, the attenuation is  $1 \times 20 \times 3 = 60$  dB, which means the amplitude ratio between the two echoes is 1,000. Similarly, a 6MHz probe would give 120 dB attenuation that is a ratio of 1,000,000. This is why high frequencies are use only to scan organs that are close to the probe. Generally speaking, in ultrasonography, a compromise needs to be found between a high frequency, which is desirable to get a good resolution, and a low frequency to get a good penetration.

## 2.2.2 Ultrasounds in the body

### The body as an acoustic medium

Table 1 summarizes the acoustic characteristics of human tissues (data from the compilation by Goss et al. [8, 9] and [10]). In reality, these values depend on the temperature of the medium and measuring conditions. In addition, several other less quantifiable factors can influence them, such as the age and the healthy or pathological state of the organs.

Several values are worth noticing:

- The acoustic properties of air are very different from those of water or biological tissues.
- All biological tissues — except lungs, since they contain air, and bones — have very close acoustic properties, and are referred to as soft tissues. Moreover, these values are similar to those of liquids such as water and blood.
- Air, bones and lungs strongly attenuate ultrasounds. Therefore, these elements constitute obstacles to ultrasound examinations.

### Interfaces

Table 2 give a few examples of amplitude and energy reflection coefficients corresponding to typical interfaces in ultrasound imaging.

Medium	Density [ $\text{kg} \cdot \text{m}^{-3}$ ]	Speed of sound [ $\text{m} \cdot \text{s}^{-1}$ ]	Characteristic acoustic impedance [ $\text{kg} \cdot \text{m}^{-2} \cdot \text{s}^{-1}$ ]	Attenuation $\alpha$ at 1 MHz [ $\text{dB} \cdot \text{cm}^{-1}$ ]
Air	1.2	333	$0.4 \times 10^3$	12
Blood	$1.06 \times 10^3$	1566	$1.66 \times 10^6$	0.2
Bone	$1.38 - 1.81 \times 10^3$	2070 – 5350	$3.75 - 7.38 \times 10^6$	10
Brain	$1.03 \times 10^3$	1505 – 1612	$1.55 - 1.66 \times 10^6$	0.6
Fat	$0.92 \times 10^3$	1446	$1.33 \times 10^6$	0.48
Kidney	$1.04 \times 10^3$	1567	$1.62 \times 10^6$	
Lung	$0.40 \times 10^3$	650	$0.26 \times 10^6$	40
Liver	$1.06 \times 10^3$	1566	$1.66 \times 10^6$	0.5
Muscle	$1.07 \times 10^3$	1542 – 1626	$1.65 - 1.74 \times 10^6$	1.09
Spleen	$1.06 \times 10^3$	1566	$1.66 \times 10^6$	
Water	$1.00 \times 10^3$	1480	$1.48 \times 10^6$	0.0022
Soft tissues		1540 (avg)	$1.63 \times 10^6$	0.54 (avg)

Table 1: Approximate densities, sound speeds, characteristic acoustic impedances and attenuation of human tissues.

Interface	Amplitude ratio $A_r/A_i$	Reflected energy (%)
Fat - muscle	0.10	1.08
Muscle - blood	0.03	0.07
Bone - Fat	0.69	48.91
Soft tissues - water	0.05	0.23
Soft tissues - Air	0.9995	99.9
Skin - piezoelectric element	0.89	80

Table 2: Reflection coefficients in the case of normal incidence.

- The soft tissue - water interface is almost not reflective. This is why ultrasound examination of a body immersed in water yield give good images.
- However, the soft tissue - air interface is very reflective. Air must be eliminated to get a decent ultrasound image. Scanning the lungs is impossible, except in certain cases where water presence is expected.
- The skin - piezoelectric element interface is also very reflective. The protective layer in front of active elements is quarter-wave, which improves the transmission. The use of a liquid gel to make the transition between the probe and the skin avoids the formation of air bubbles.
- The bone - fat interface is quite reflective compared to interfaces between soft tissues. Scanning bones results in hyperechogenic zones on the image, which correspond the the bone surface. Moreover, the bone transmits almost no energy, which results in no perceptible signal beyond the bone.

## 2.3 Reconstructing the ultrasound signal

In order to highlight the pertinent information and display it on an image, the signal coming out of the receiving transducer needs to be processed. The steps of the process are summarized in figure 6 and described below.

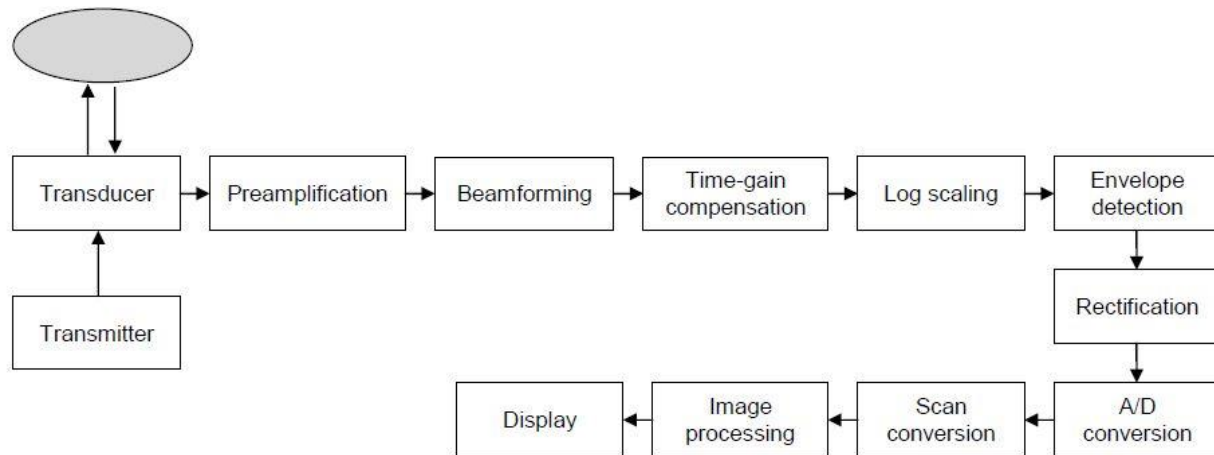


Figure 6. RF signal processing

## Ultrasonic transmitter

The role of the transmitter is to excite the transducer in order to generate a short pulse, for example, a unipolar pulse of -200V in 10 ns.

## Beamforming

The electronic beam steering and focusing requires delay lines, that can be implemented in two different ways:

- The delay lines are passive LC circuits with fixed values. Focusing is then performed at a fixed depth.
- Dynamic focusing can be performed with programmable delay lines.

## Time gain compensation

Due to attenuation, two identical reflectors located at different depths would not yield echoes of equal amplitude, because the path taken by the wave is different in both cases. This difference can be approximately corrected by time gain compensation, which consists in amplifying the signal with a gain that increases over time. The gain variation can reach 60 to 70 dB while maintaining a dynamic range of 40 db. The attenuation function of a given environment cannot be perfectly known, so the TGC function needs to be tweaked to adapt to the observed image. The compensation is therefore always approximate, and no quantitative data on acoustic properties can be extracted from an ultrasound image.

## Logarithmic scaling

In ultrasonography, we need to visualize very strong echoes coming from highly reflective obstacles, such as bones or air, and very weak echoes at the same time. The dynamic range of the RF signal is on the order of 100 dB, whereas the dynamic range that the human eye can perceive is only about 30 dB. By applying a logarithmic scaling to the signal, a wider range of gray is used to represent less echogenic zones, thus enhancing the image contrast in these areas. Highly echogenic zones have fewer gray levels, but this is not a problem since they only correspond to walls or organ boundaries.

## Envelope detection

The ultrasound image construction only uses the amplitude of the received signal. The phase information is dismissed. The amplitude information is extracted from the RF signal by an envelope detector, which demodulates the signal by removing the high-frequency carrier wave, that is, oscillations of the same frequency as the transducer.

## Analog to digital conversion

In order to be processed and stored, the signal is digitized. An 8-bit quantization is generally used.

## Scan conversion and display

The data collected by the scanner correspond to a series of echoes coming from each line of exploration. These lines do not necessarily have the same orientation, especially in the case of sector scanning. A scan conversion needs to be done to convert polar coordinates into Cartesian coordinates, so that the image can be displayed on a monitor.

# 2.4 Modes of sonography

Three imaging modes are usually used in clinical routine: the M-mode, the B-mode and the Doppler mode.

## 2.4.1 M-mode

M stands for motion. The M-mode consists in continuously observing the echoes generated by an

ultrasound beam, whose spatial orientation is fixed. The echoes received by the probe vary according to the movement of organs crossed by the beam. An M-mode image is obtained by displaying the variation of echoes in position and intensity over time. As only one spatial dimension is covered, the time resolution with this method is much higher than in B-mode, which allows the observation of very fast movements. For instance, M-mode is often used in echocardiography to observe the movements of heart walls and valves.

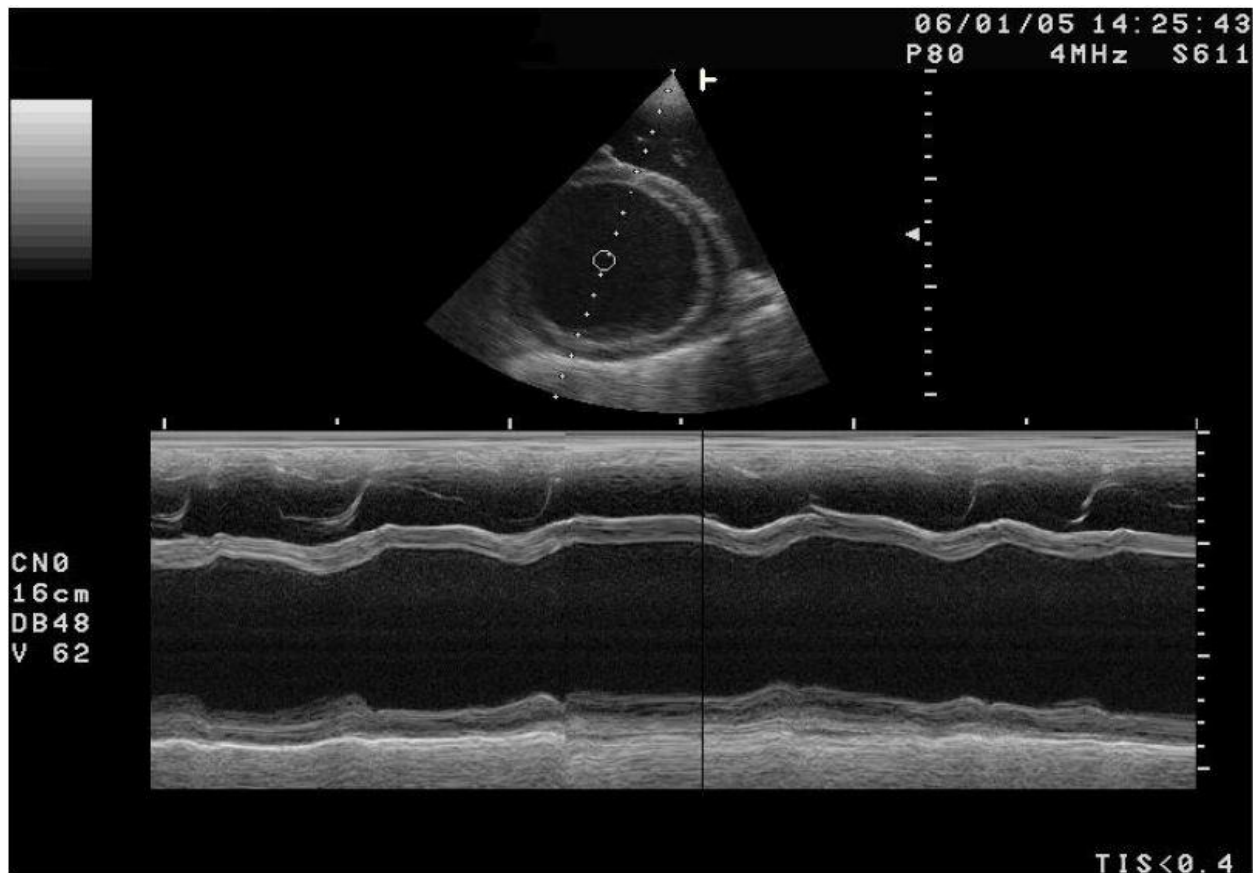


Figure 7: M-mode and B-mode images. (top) B-mode image representing a heart section. (bottom) M-mode representation of the dotted line (Source: <http://de.wikipedia.org/wiki/Kardiomyopathie>)

## 2.4.2 B-mode

B-mode is the most widespread mode in clinical routine. It consists in scanning a plane through the body and displaying the received echoes in a two-dimensional image. To do so, many emissions are done successively, each time with a different beam orientation. The position of an echo on the image is determined by its travel time and the corresponding beam orientation. The acquisition process is quite fast and generally allows a framerate of 20 to 30 images per second.

### 2.4.3 Doppler mode

Medical ultrasound scanners can also be used for visualizing the blood flow dynamically in the body. The so-called Doppler systems can interrogate the flow at a single position in the body and find the velocity distribution over time. Measurements are performed by repeatedly pulsing in the same direction and then use the correlation from pulse to pulse to determine the velocity.

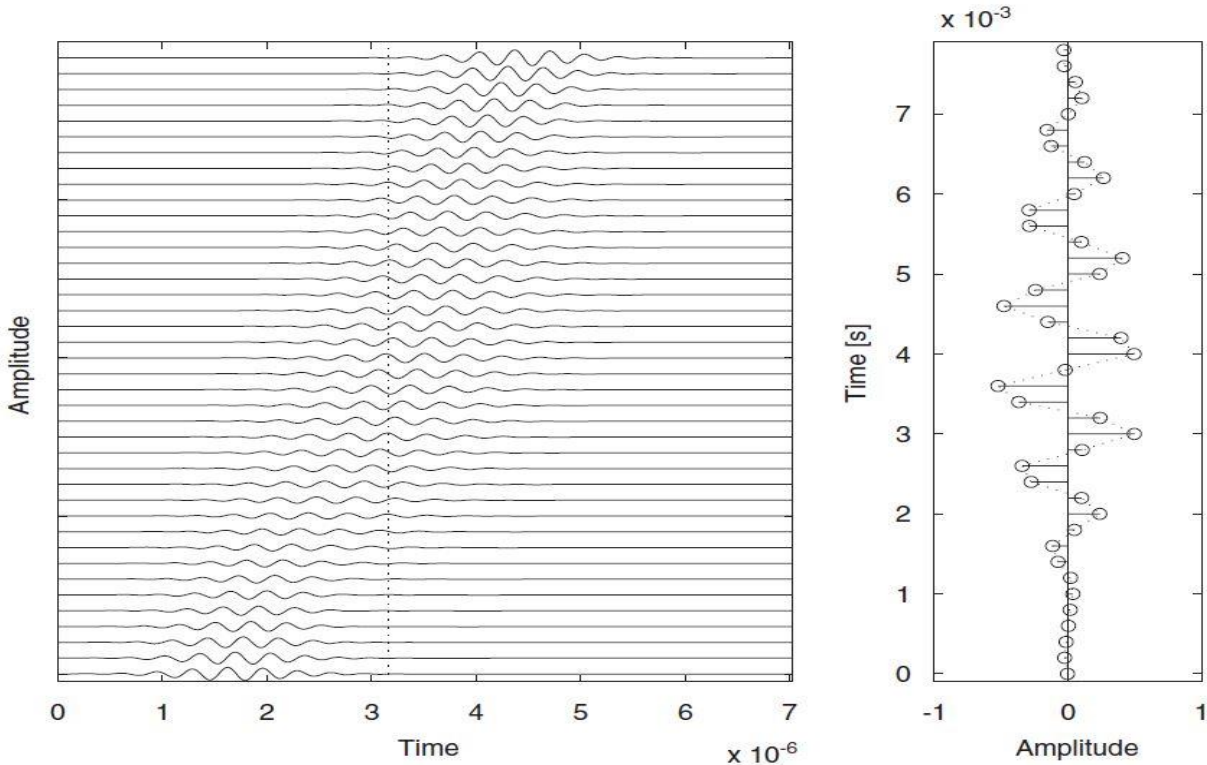


Figure 8: RF sampling of single pulse moving away from the transducer. The left graph shows the different received RF lines, and the right graph is the sampled signal. The dotted line indicates the time when samples are acquired

### Measurements of flow signals

The data for the velocity measurement are obtained by emitting a short ultrasound pulse with 4-8 cycles at a frequency of 2-10MHz. The ultrasound is then scattered in all directions by primarily the blood cells and part of the scattered signal is received by the transducer and converted to a voltage signal. The blood velocity is found through the repeated measurement at a particular location. The blood cells will then pass through the measurement gate and give rise to a signal with a frequency proportional to velocity as [7]



$$f_p = \frac{2v_z}{c} f_0$$

where  $f_0$  is the emitted ultrasound frequency,  $v_z$  is the blood velocity along the ultrasound beam, and  $c$  is the average speed of sound in soft tissues. A simple model for the sampled signal  $r(i)$  emanating from a single moving scatterer as shown in figure 2.8 is

$$r(i) = g(i) \sin \left( 2\pi \frac{2v_z}{c} f_0 i T_{prf} - \theta \right)$$

where  $i$  is the number for the emitted pulse and  $\theta$  is a phase shift introduced by the propagation time in the tissue.

The sampling time is  $i T_{prf}$  and the frequency of the received signal is scaled by the factor  $2v_z/c$  and is directly proportional to velocity. A higher velocity will make the pulse in Fig. 8 move faster past the sampling point and compress the pulse yielding a higher frequency and a lower velocity will lengthen the pulse and lower the frequency. The velocity can, thus, be estimated from the mean frequency in the received signal.

The velocity can be both towards and away from the transducer, and this should also be included in the estimation of velocity. The sign can be found by using a pulse with a one-sided spectrum corresponding to a complex signal with a Hilbert transform relation between the imaginary and real part of the signal. The one sided spectrum is then scaled by  $2v_z/c$  and has a unique peak in the spectrum from which the velocity can be found. The complex signal can be made by Hilbert transforming the received signal and using this for the imaginary part of the signal.

## Spectral velocity estimation

Using a number of pulse-echo lines and sampling at the depth of interest, thus, gives a digital signal with a frequency proportional to velocity. Having a movement of a collection of scatterers with different velocities then gives a superposition of the contribution from the individual scatterers and gives rise to a spectral density of the signal equal to the density of the velocities. Making a Fourier transform on the received signal will, thus, directly reveal the velocity distribution for a given time.

# Chapter 3

## Super resolution

### 3.1 Theory and Background

In many imaging systems, however, the quality of image resolution is limited by physical constraints. The imaging systems yield aliased and under sampled images if their detector array is not sufficiently dense. So, digital image processing approaches have been investigated to reconstruct a high-resolution image from multiple degraded low-resolution images. Actually, by using super resolution algorithms, high resolution images can be reconstructed from a series of low resolution images and the idea behind this concept is to combine the information from a set of undersampled(aliased) low resolution images of the same scene and use it to construct a high resolution image or image sequence [11].

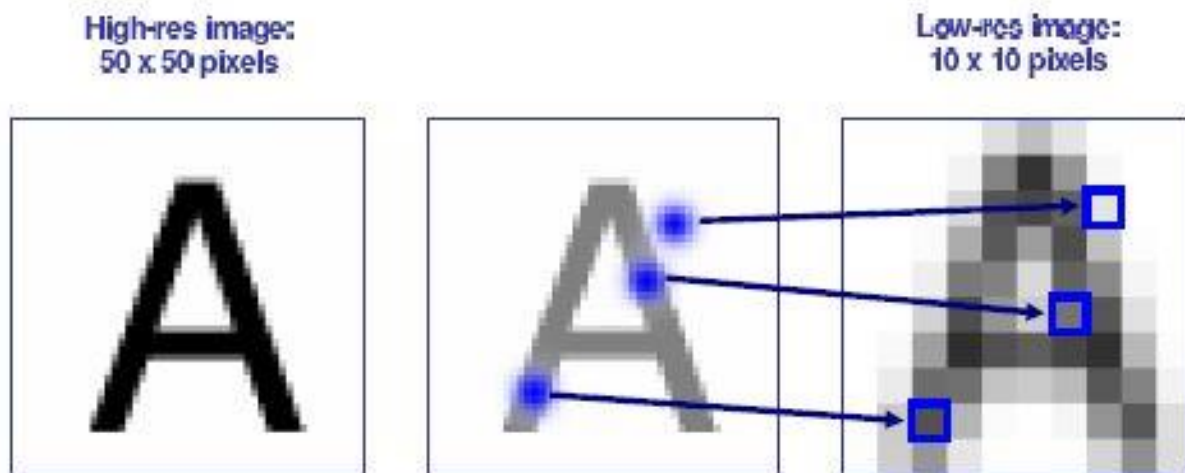


Figure 9: The creation of low-resolution image pixels. The low-resolution image on the right is created from the high-resolution image on the left one pixel at a time. The locations of each low-resolution pixel are mapped with sub-pixel accuracy into the high-resolution image frame to decide where the blur kernel (plotted as a blue Gaussian in the middle view) should be centered for each calculation.

Each low-resolution pixel can be treated as the integral of the high-resolution image over a particular blur function, assuming the pixel locations in the high-resolution frame are known, along with the point-spread function that describes how the blur behaves. Since pixels are discrete, this

integral in the high-resolution frame is modelled as a weighted sum of high-resolution pixel values, with the point-spread function (PSF) kernel providing the weights. This image generation process is shown in Figure 1.4. Each low-resolution pixel provides us with a new constraint on the set of high-resolution pixel values. Given a set of low-resolution images with different sub-pixel registrations with respect to the high-resolution frame, or with different blurs, the set of constraints will be non-redundant. Each additional image like this will contribute something more to the estimate of the high-resolution image.

In addition to the model of Figure 9, however, real sensors also have associated noise in their measurements, and real images can vary in illumination as well as in their relative registrations. These factors must also be accounted for in a super resolution model, so the full picture of how a scene or high-resolution image generates a low-resolution image set looks more like that of Figure 10.

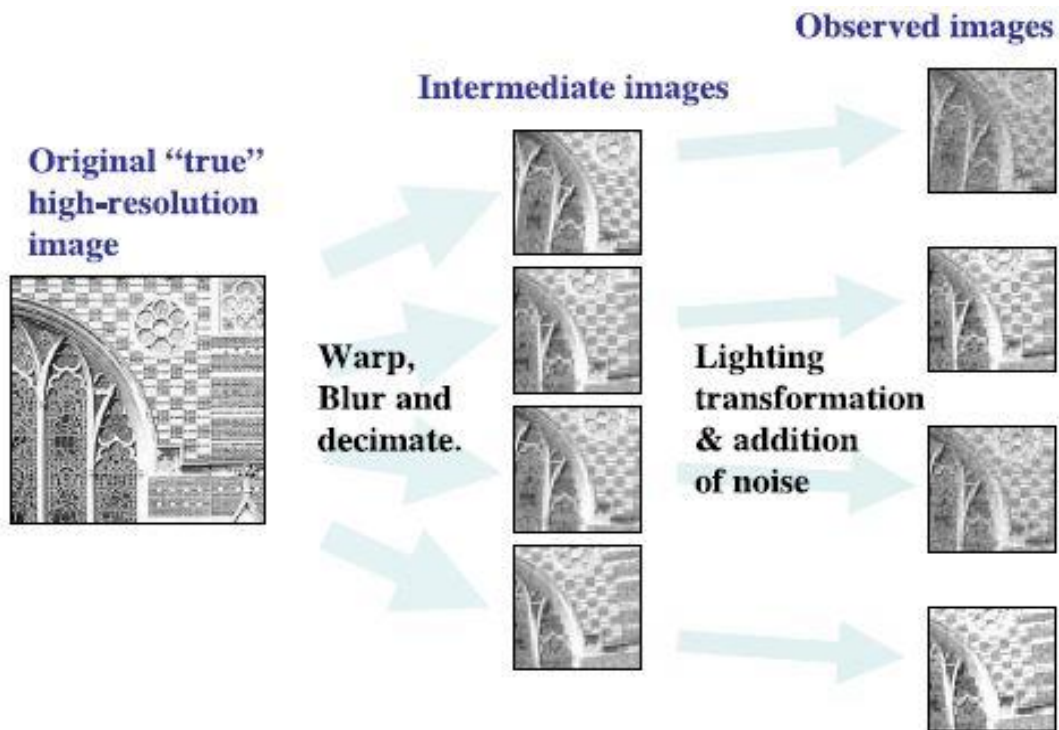


Figure 10: One high-resolution image generates a set of low-resolution images. Because the images are related by sub-pixel registrations, each observation gives us more additional constraints on the values of the high-resolution image pixel intensities.

Many reconstruction methods have been proposed over the years but, most super resolution reconstruction methods employ following steps: image registration, interpolation and optional restoration (deblurring, denoising). Some methods perform these tasks separately, while others combine two or more of them.

## 3.2 Early super-resolution methods

In following we would have a take a look at historical improvement of super resolution technique.

### 3.2.1 Super resolution in frequency domain

Tsai and Hung were the first to consider the problem attaining a high resolution image from mixing a set of low resolution images. Their data set had been achieved by Landsat Satellite photographs. They modelled the images as aliased translationally displaced versions of a constant scene. They had been used from discrete time Fourier transform in their method. It can be said that their approach was based on the 3 following items:

1. Shifting property of the Fourier Transformation.
2. Aliasing relationship between continuous Fourier transform and high resolution image.
3. Band limited high resolution image. Figure 11 represent aliasing relationship between low resolution image and high resolution image.

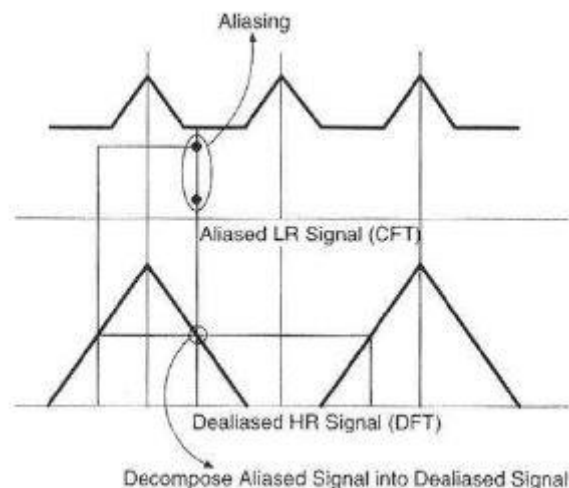


Figure 11 :Aliasing relationship between LR and HR image. This figure is from [16]

But, they did not consider noise and optical blur in their method. Ozkan, Tekalp and Sezan by using noise and point spread function, extended Tsai and Haung formulation. Kim, Bose and Valenzuelan also used the model of Tsai and Haung but with consideration of noise and blur. The drawback with their technique was that because of presence of zeroes in the PSF, this method was ill-posedness. Moreover, the motion estimation was not considered in their method.

### 3.2.2 Spatial domain methods

Actually, most of research that has been done in super resolution field is in this class of reconstruction methods and the reason for that is firstly, the constraints are much easier to formulate and secondly, this technique include a great flexibility in in the motion model, motion blur, optical blur and the sampling process.

### 3.2.3 Projection and interpolation

If ideal sampling is considered, then our issue reduces essentially to projection a high resolution grid and interpolating of non uniformly spaced samples. Comparison between different interpolation methods with high resolution reconstruction results can be found in [12] and [13].

### 3.2.4 Probabilistic methods

Modelling of images as probability distribution seems to be acceptable because super resolution has been relying on the approximation of parameters and data that are unknown. Schultz and Svensson [14] used Huber Markov random fields in Bayesian framework to clarify discontinuity preserving prior image density function. MAP estimation that relate on to independent motion is done by gradient projection algorithm is considered. Motion estimation error is also considered as probability density function.

Hardie, Barnard and Armstrong also followed the Schultz and Svensson but, they made a difference by estimating the high resolution image and motion parameters at the same time. In fact, their work had the advantage of of not estimating motion directly from low resolution images.

Moreover, Tom and Katsaggelos [15] instead of MAP approach used ML method to reduce blur

and noise. By utilizing exception maximization technique they can obtain registration and restoration concurrently.

### 3.2.5 Iterative method

The iterative methods are the most important technique in spatial domain methods. The benefits of this technique is the possibility of dealing with vast range of data(images)sequence, easy inclusion of spatial domain and the capability of this technique to utilizing varying degradation. Actually, by the iteration technique first of all we make a rough guess and then try to achieve successfully more developed estimation.

As a matter of fact, there are so many iterative techniques to solve super resolution reconstruction methods.

Feuer and Elad use different approximation to the Kalman filter and estimate its performance by Recursive Least Square (RLS), Least Mean Square (LMS) and Steeped Descent (SD). Irani and Peleg introduced the Iterative Back Projection (IBP) algorithm oriented from computer aided tomography (CAT).

To decrease the ill posedness and noise Stack et.al. Applied a set of theoretic algorithm projection on to convex sets (POCS). Peleg and Irani modify their method to deal with more complex motion types like local motion partial occlusion and transparency. Shah and Zakhor also followed the Peleg and Irani and proposed a novel approach for motion estimation.

### 3.2.6 Projection on to convex sets

This technique is an alternative iterative method to have a feature based on prior knowledge about possible solution into the reconstruction process. Actually this approach approximates the super resolution image based on finding solution for the problem of interpolation and restoration.

This method was first introduced by Oskoui and stark[17].They used from convexity and closeness of the constraint sets to ensure convergence of iterativity projecting the images on to the sets; but their solution has some drawbacks. For example, it was dependence of initial guess and it was non-unique.

Takalp et.al. Then used from Oskoui and Stark formulation and make that more robust by

considering the observation noise and the motion blur [18]. Based on the POCS method incorporating a priori knowledge into the solution can be represented as a limit to solution to be a member of a closed convex set  $c_i$  which can be expressed as a set of vectors that satisfy a specific property. If the limiting sets have a non-empty intersection, then a solution that belongs to the intersection set  $c_s$  can be found by projections onto those convex sets.

The advantage of POCS method is that it uses from strong spatial domain observation model. Moreover, its simplicity and flexibility should not be ignored. Furthermore, some problems with this technique is having a high computational cost, slow convergence and non-uniqueness [1].

Peleg and Irani modify their method to deal with more complex motion types like local motion partial occlusion and transparency. Shah and Zakhor also followed the Peleg and Irani and proposed a novel approach for motion estimation.

### 3.2.7 Edge-preservation method

Milanfar et.al. Proposed using the  $L_1$  norm in the super resolution both for data fusion and for the image registration.  $L_1$  Norm has the capability of removing outlier efficiently. Moreover, it performs spatially well in facing with non-Gaussian noise. Furthermore, the results that achieved by  $L_1$  norm approach are less sensitive to the outlier in the super resolution images.

## 3.3 Challenges

Super-resolution algorithms face a number of challenges in parallel with their main super-resolution task. In addition to being able to compute values for all the super resolution image pixels intensities given the low-resolution image pixel intensities, a super resolution system must also be able to handle:

- Image registration – small image displacements are crucial for beating the sampling limit of the original camera, but the exact mappings between these images are unknown. To

achieve an accurate super-resolution result, they need to be found as accurately as possible.

- Lighting variation – when the images are aligned geometrically, there may still be significant photometric variation, because of different lighting levels or camera exposure settings when the images were captured.
- Blur identification – before the light from a scene reaches the film or camera CCD array, it passes through the camera optics. The blurs introduced in this stage are modelled by a point-spread function. Separating a blur kernel from an image is an extensively-studied and challenging problem known as Blind Image Deconvolution. This can be even more challenging if the blur varies spatially across the image.

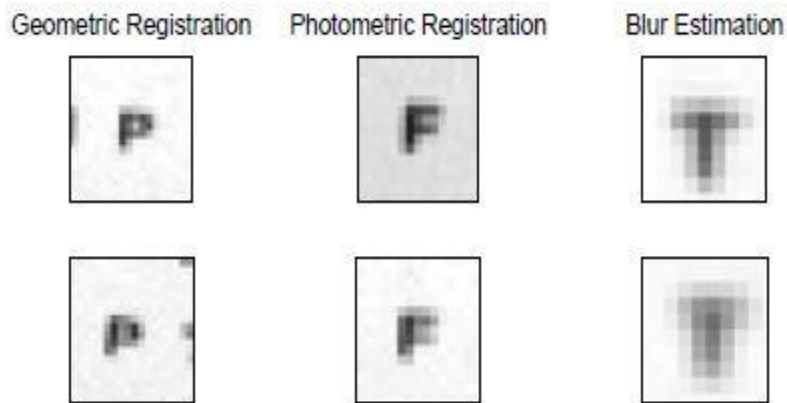


Figure 12: Three of the challenges facing a multi-frame super-resolution algorithm. Left column: the two instances of the “P” character have different alignments, which we must know accurately for super-resolution to be possible. Middle column: the eyechart in the images has different illumination between two frames, so the photometric registration between the images also has to be estimated. Right column: the image blur varies noticeably between these two input frames, and blur estimation is a difficult challenge.

These three cases are illustrated for some low-resolution image patches in Figure 12. While the goal is to compute a high-resolution image, the efficacy of any super-resolution approach depends on its handling of these additional considerations as well. Given “good” low-resolution input images, the output from an otherwise successful super-resolution algorithm will still be poor if the registration and blur estimates are inaccurate.



# Chapter 4

## Compressive Sensing

### 4.1 Compressive Sensing Theory

#### 4.1.1 Background: The drawback of Nyquist sampling

According to the Shannon/Nyquist sampling theorem, in order to reconstruct a bandlimited signal perfectly the sampling rate should be at least two times that of the signal bandwidth [19]. To be more specific, let  $x(t)$  represent a continuous-time signal and  $x(f)$  be the continuous Fourier transform of the signal  $x(t)$ , we have:

$$x(f) = \int_{-\infty}^{\infty} x(t)e^{-i2\pi ft} dt$$

The signal  $x(t)$  is said to be bandlimited if there is a  $B$ , such that  $x(f)=0$  for all  $|f| > B$ . Figure 13 shows an example of a bandlimited signal  $x(t)$ . The quantity  $2B$  is called the Nyquist rate. The sufficient condition for signal  $x(t)$  to be perfectly reconstructed from an infinite sequence of samples is the sample rate  $f_s$  should be larger than  $2B$ . If  $f_s$  is less than  $2B$ , aliasing will be introduced after reconstruction.

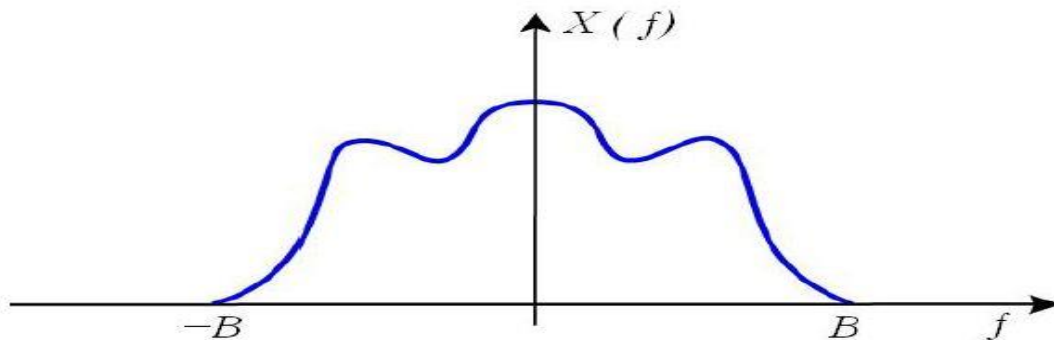


Figure 13: An example the Fourier transform of a bandlimited signal  $x(t)$  [3]

While in reality, this sampling rate is still so high that too many samples should be achieved. Especially in the medical imaging modality, we need to reduce the time of the patients' exposure in the electromagnetic radiation. So it is desirable to take as few samples as possible without losing essential information. It is interesting to notice that most signals in reality are sparse. When they are represented in some domain (such as the wavelet domain), they contain many coefficients close to or equal to zero. Compressed sensing acquires and reconstructs a signal applying the prior knowledge that it is sparse. It can capture and represents compressible signals at a rate significantly lower than Nyquist rate.

### 4.1.2 The sparsity of signals

Using mathematics to illustrate, we have a discrete-time signal  $x$  in  $\mathbb{R}^N$  that can be represented in terms of an orthonormal basis of  $N \times 1$  vectors  $[\Phi]_{i=1}^N$  as follows:

$$X = \sum_{i=1}^N s_i \Phi_i \quad (1)$$

Where  $s_i$  is the coefficient sequence of  $X$ . For simplification, we can write (1) in matrix form as  $X = \Phi s$  (where  $S$  is the  $N \times 1$  column vector  $\Phi$  and is the matrix with  $\Phi_i$  as columns). Signal  $X$  has a  $K$ -sparse expansion if only  $K$  of the entries in  $S$  are non-zero and  $(N-K)$  are zero. Real signals are often compressible which means the sequence of coefficients decays quickly. It means the large fraction of small coefficients can be thrown away without much perceptual loss.

### 4.1.3 The inefficiencies of conventional data transform

In traditional data acquisition, the first step is to acquire the full  $N$ -sample signal; then compute the coefficients  $\{s_i\}$  via  $s = \Phi^T X$  and only keep the  $K$  largest  $\{s_i\}$  while discarding the others. The values and locations of the  $K$  largest  $\{s_i\}$  should be encoded. This traditional signal acquisition processing divides the sampling and compression into two separate processes which samples a lot of unnecessary information. This inefficiency is more obvious when the number of samples  $N$  is large compared to  $K$ . Compressed sensing is a method to skip the sampling step by directly acquiring the compressed signal representation to overcome these inefficiencies.

#### 4.1.4 Motivation

In many settings, the signals we are working with cover only a tiny fraction of the set of all possible signals. For example, consider the case of photography and imagine a  $256 \times 256$  digital grayscale image whose pixels each obey a uniform distribution over  $[0,255]$  (Fig. 14, left). The probability of such an image being interpretable as a photograph is very close to zero. In a photograph (Fig 14, right), one would expect to see shapes, lines and textures that can be interpreted as objects, and which are very unlikely to appear in a random image.



Figure 14: Comparison of a random image (independent pixels obeying a uniform distribution over  $[0; 255]$ , on the left) and the photograph of a natural scene (portrait of Lena, on the right).

The latter observation applies to almost any type of signal: speech signal, music, MRI, seismic measurements, etc. It is also the foundation of efficient data compression. Indeed, the particular structure of a certain type of signal translates to the fact that it is possible to find a basis in which these signals have a sparse expansion, that is to say many zero coefficients. Pure sparsity is almost never attainable in practice, partly because of the presence noise, but signals are often compressible, that is to say that their coefficients in an appropriate basis decay rapidly. For example, it is now well known that most of the energy of a digitized natural image lies in very few of its wavelet coefficients. This is illustrated by Fig. 15, which compares the  $512 \times 512$  pixels portrait of Lena and a version of this portrait where only the 2621 largest wavelet coefficients (i.e. 1%) were kept and all the others set to zero.

In certain fields, data acquisition raise problems that can be difficult to get round. These difficulties can be caused by

- Physical constraints on the acquisition device, e.g. in the case of seismic data acquisition [5], cable feathering in marine surveys can lead to missing traces,
- The cost of each acquisition,
- health risks, e.g. radiation exposure in certain fields of medical imaging
- Time constraints, e.g. MRI acquisitions should be quick enough to avoid any movement of the patient, which would cause a blurred resulting image.
- The alternation between several modes of acquisition that cannot be carried out simultaneously,
- The sampling rate bound implied by the Nyquist-Shannon sampling theorem.



(a)



(b)

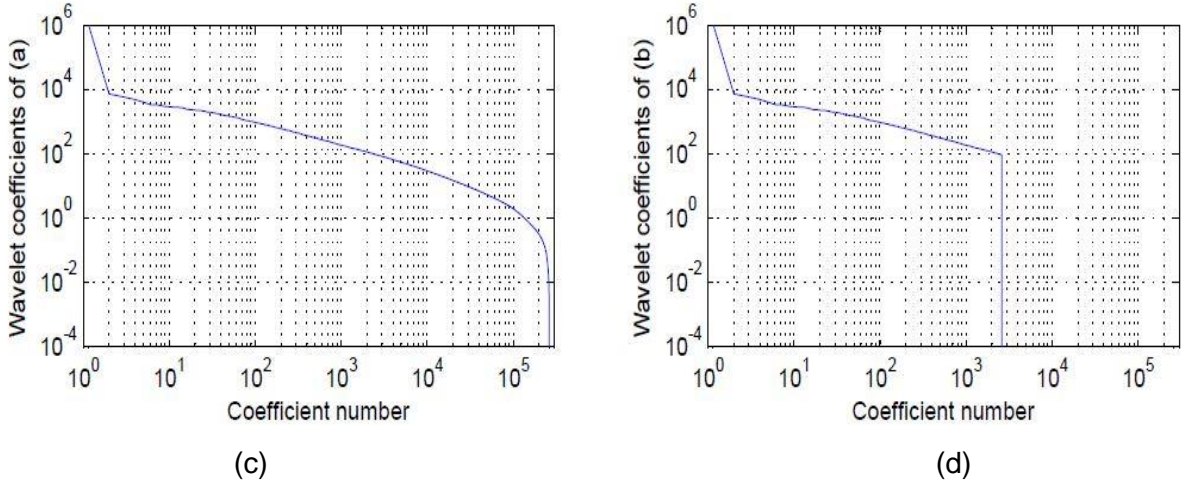


Figure 15: (a) Original  $512 \times 512$  Lena image. (b) Image reconstructed from 1% of the wavelet coefficients of the original image. Only the largest coefficients were kept. The others were set to zero. (c) Sorted wavelet coefficients of the original image. (d) Sorted wavelet coefficients of the reconstructed image.

The goal of compressive sensing [2] is to get round these problems by carrying out a limited number of measurements, from which the original signal can be reconstructed, using sparsity promoting algorithms. This method thus amounts to acquire a signal directly in a compressed form, hence the names of compressive sampling, compressive sensing or compressed sensing.

#### 4.1.5 The introduction of compressed sensing

In order to measure all the  $N$  coefficients of  $x$ , we consider  $M \times N$  ( $M < N$ ) the column inner products  $y$  between  $x$  and collection of vectors  $\{\Theta_j\}_{j=1}^M$ :

$$y = \Theta x = \Theta \Phi \hat{x} = V \hat{x} \quad (2)$$

Where  $V = \Theta \Phi$  is an matrix  $M \times N$ .  $\Theta$  is called an  $M \times N$  measurement matrix with  $\Theta_j^T$  as rows.  $\Theta$  is fixed and does not depend on the signal, so this process is non-adaptive. This is a great point since if we get a robust result from a measurement matrix  $\Theta$ , we can apply this measurement matrix  $\Theta$  to any kinds of signals without worrying about the stability. Figure 16 illustrates the process of compressed sensing.

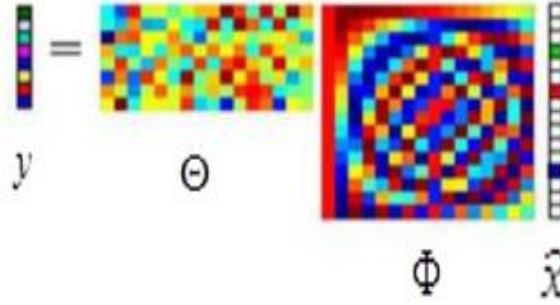


Figure 16: A Pictorial representation of CS process [3]

## 4. 2 Conditions for successful CS signal recovery

Successful CS signal recovery is possible under two conditions. Firstly, the signal to be recovered has to be sparse, or at least compressible, in the domain described by  $\Phi$ . Secondly, the signal must be “mixed” sufficiently during the acquisition process. The mixing depends on the coherence between  $\Theta$  and  $\Phi$  on one hand, and on the randomness of the sampling scheme on the other hand.

### 4.2.1 Restricted isometry property (RIP)

The main task of encoding is to transform the  $N \times 1$   $K$ -sparse signal  $x$  to the  $M \times 1$  measurement  $y$  by using a proper measurement matrix  $\Theta$ . The sampling matrix  $\Theta$  must map two different signals to two different sets of measurements, so all of the column submatrices (containing at most  $K$  columns) of should be well-conditioned.

Candès and Tao proposed a condition for the sampling matrix  $\Theta$ . For all  $K$ -sparse vector  $x$ , an  $M \times N$  matrix  $\Theta$  has the  $K$ -restricted isometry property if

$$(1 - \delta_k) \|X\|_2^2 \leq \|\Theta X\|_2^2 \leq (1 + \delta_k) \|X\|_2^2 \quad (3)$$

When  $\delta_k$  is less than 1, the inequalities (3) imply the all of the submatrices of  $\Theta$  with  $K$  columns are well-conditioned and close to an isometry. If  $\delta_k \ll 1$ , the sampling matrix  $\Theta$  has a large probability to reconstruct the  $(K/2)$ -sparse signal  $X$  stably.

This condition is called Restricted Isometry Property (shorted for RIP). The connection between RIP and Compressed Sensing is if  $\delta_{2K}$  is sufficiently less than 1, all pairwise distances between K-Sparse signals must be well preserved in the measurement space which implies that  $(1 - \delta_{2K})\|X_1 - X_2\|_2^2 \leq \|\Theta X_1 - \Theta X_2\|_2^2 \leq (1 + \delta_{2K})\|X_1 - X_2\|_2^2$  holds for all K-sparse vectors  $X_1$  and  $X_2$ . Because  $X_1$  and  $X_2$  are two different vectors and  $\|X_1 - X_2\|_2^2$  are always larger than zero,  $\|\Theta X_1 - \Theta X_2\|_2^2$  will never equal to zero. It can be said that the sampling matrix  $\Theta$  should map two different K-sparse signals to different samples.

So as to invert the sampling process stably and get a K-sparse signal X, we need to get a small restricted isometry constant  $\delta_{2K}$ . However, it is computational difficult to check whether a matrix  $\Theta$  satisfies the inequality (3). Fortunately, many types of random matrices have a good restricted isometry behavior, and they satisfy the restricted isometry condition with high probability. One of the quintessential examples is Gaussian measurement matrix  $\Theta$  that the entries  $\Theta_j$  of  $\Theta$  are independent and identically distributed (i.i.d.) random variables from a Gaussian probability density function. An M X N i.i.d. Gaussian matrix has restricted isometry behavior with high probability if  $M \geq c \cdot K \cdot \log(N / K)$  where  $c$  is a constant [2] [4]. This also means K-spare or compressible signals with length N can be recovered with M random Gaussian measurements.

## 4.2.2 The idea of Reconstruction

In order to achieve an optimal recovery algorithm, there are several requirements that should be satisfied. The requirements are illustrated as below:

- (1) Stability. The algorithm should be stable. That means when the signals or the measurements are perturbed slightly by noise, recovery should still be approximately accurate.
- (2) Fast. The algorithm should be fast if we want to apply it into practice.
- (3) Uniform guarantees. When acquiring linear measurements by using a specific method, these linear measurements can apply to all sparse signals.

(4) Efficiency. The algorithm should require as few measurements as possible.

Now we want to reconstruct a  $K$ -sparse signal  $x \in \mathbb{R}^N$  by the  $M \times N$  measurement vector  $y = \Theta x$ . Since the measurement matrix  $\Theta \in M \times N$  and  $M < N$ , the system (2) is underdetermined. That means we have more unknowns than the equations. Theoretically, there are infinitely many  $\hat{x}$  that satisfy Eq. (2). However, in our case the additional assumption is that  $x$  is  $K$ -sparse, and then there is often a unique  $\hat{x}$  that will suffice to recover  $y$ . The best solution will be the sparsest vector that means it has the most zero coefficients. Consider the  $l_0$  norm that counts the number of non-zero entries, the reconstruction problem turns to be:

$$x = \arg \min_{\hat{x}} \|\hat{x}\|_0, \text{ subject to } y = \Theta \hat{x} \quad (4)$$

Unfortunately, the  $l_0$ -minimization problem is NP-hard [29] [30]. It is computationally intractable to solve Eq. (4) for any matrix and vector. There are two families can be alternatively used to solve Eq. (4). One is the basic pursuit that is a convex relaxation leading to  $l_1$ -norm minimization [25], the other is greedy pursuit [20] such as Orthogonal Matching Pursuit (OMP) [24], Stagewise Orthogonal Matching Pursuit (StOMP) [26], and Regularized Orthogonal Matching Pursuit (ROMP) [27][28].

### $l_1$ -minimization approach

As we discussed in section 4.2.1(RIP), in most cases if the RIP holds, the  $l_1$  norm can exactly recover  $K$ -sparse signals and do a proper job to approximate the compressible signals with high probability using only  $M = O(K \cdot \log(N / K))$  i.i.d. Gaussian measurements. Then the Eq. (4) will change to be:

$$x = \arg \min_{\hat{x}} \|\hat{x}\|_1, \text{ subject to } y = \Theta \hat{x} \quad (5)$$

Eq. (5) is equivalent to the linear programming

$$\min \sum_{j=1}^{2N} v_j, \text{ subject to } V \geq 0, y = (\Theta, -\Theta)V \quad (6)$$

Where  $V$  is a positive real number of size  $2N$ . The signal  $X$  is obtained from the solution  $V^*$  of (6) via  $X = (I, -I)V^*$ . So the  $l_1$  norm minimization can be solved by linear programming problem.



Interior-point methods [21], projected gradient methods [22] and iterative thresholding [23] can be used to solve the Eq. (6).

The  $l_1$  minimization approach can provide stability and uniform guarantees. But it doesn't have linear bound on the runtime, it is not optimally fast. The basic pursuit is well developed and I am not going to talk too much about it. Greedy pursuit is the target I will focus on.

### 4.2.3 Greedy pursuit

Greedy pursuit is another approach to reconstruct the signal. It is an iterative signal recovery algorithm to calculate the support of the signal and it makes the locally optimal choice at each time to build up an approximation and repeats until the criterion is fulfilled. When we get the support  $S$  of the signal, the signal  $x$  can be reconstructed by  $x = (\Theta_s)^\dagger y$ , where  $\Theta_s$  is the measurement matrix  $\Theta$  with entries indexed by  $S$  and  $(\Theta_s)^\dagger$  is the pseudoinverse of  $\Theta$ . The pseudoinverse of a full-rank matrix  $\Theta$  is defined by the formula  $\Theta^\dagger = (\Theta^* \Theta)^{-1} \Theta^*$ .

Greedy pursuit is extremely fast while it is not optimally stable and doesn't have uniform guarantees.

## Chapter 5

### Implementation

The theory of CS heavily depends on signal or image sparsity and can efficiently extract the most efficient information from a small number of measurements, i.e., to reduce the collection of inessential data [31] [3]. CS demonstrates that a small non-adaptive linear measurements of a compressive image have enough information to reconstruct it perfectly [31] [32]. If we represent our desired high-resolution image as an  $n$ -dimensional vector  $x \in R^n$  where  $n$  is large. We want to estimate this high-resolution signal from the low-resolution input  $y \in R^m$ , where  $m \ll n$ . Let us consider that signal  $y$  has been acquired from the original through a linear down sampling measurement process, represented as

$$y = \Theta x \quad (7)$$

Where  $x$  is an  $n \times 1$  high-resolution image vector in spatial domain,  $\Theta$  is a sampling matrix that performs the linear measurements on  $x$ . Our goal is to recover the high-resolution  $x$  using only  $y$  as input.

Initially, this seems like an impossible feat since the  $m$  samples of  $y$  yield a  $(n - m)$  dimensional subspace of possible solutions for the original  $x$  that would match our given observations. In order to know one of those possible solutions for our desired  $y$  we apply a key assumption of CS that transformed version of signal,  $\hat{x}$  is  $k$ -sparse under some basis  $\Phi$ , it means that at most  $k$  non-zero coefficients in that basis (e.g.,  $\|\hat{x}\|_0 \leq k$ , where  $\|\cdot\|_0$  denotes the  $l_0$  quasi-norm). This is not an unreasonable assumption, since we know that the high-resolution image will be a real world image, and so it will be compressible in a transform domain, e.g., wavelet transform. We can now write our measurement process from Eq. (7) as:

$$y = \Theta \Phi \hat{x} = V \hat{x} \quad (8)$$

where  $V = \Theta \Phi$  is a general  $m \times n$  measurement matrix. If we can have for  $\hat{x}$  given the measured  $y$ , to get our desired high resolution signal  $x$  we could apply the inverse transform  $\Phi^* x$ . Unfortunately, conventional techniques such as least square, inversion approach for solving for  $\hat{x}$  do not work since Eq. (8) is severely under-determined. However, in paper[1] proof show that in CS if  $m \geq 2k$  and  $V$  meets certain properties of the restricted isometry property (RIP)[33], that is:

$$(1 - \delta_k) \|\alpha\|_2 \leq \|V\alpha\|_2 \leq (1 + \delta_k) \|\alpha\|_2, (0 < \delta_k < 1) \quad (9)$$

where  $\alpha$  represents random  $k$ -sparse vector. In general, the RIP states that a measurement matrix will be valid if every possible set of  $Z$ -sparse vector columns of  $V$  forms an approximate orthogonal set. In effect, we want the sampling matrix  $\Theta$  to be as incoherent to the compression basis  $\Phi$  as

possible. Examples of matrices that have been proven to meet RIP include Gaussian matrices, partial Fourier matrices and Bernoulli matrices [34].

Then Eq.(8) can be solved uniquely for the sparsest  $\hat{x}$  that satisfies the equations in paper[1].Therefore the sparse solution for Eq.(8) is found by solving the following  $l_0$  norm minimization problem,

$$\min \|\hat{x}\|_0 \text{ s.t. } y = V\hat{x} \quad (10)$$

Where  $\|\hat{x}\|_0$  describes the  $l_0$  norm, the number of non-zero entries in  $\hat{x}$ . The solution to the problem in Eq. (10) is combinatorial in nature with prohibitive computational load in practical applications. Convex relaxation of the  $l_0$  problem to the following  $l_1$  problem,

$$\min \|\hat{x}\|_1 \text{ s.t. } y = V\hat{x} \quad (11)$$

The  $l_1$  optimization of Eq. (11) will solve correctly for  $\hat{x}$  [41] as long as the number of samples  $m = O(k \log n)$  and the matrix  $V$  meets the RIP [33] with this parameters  $(2k, \sqrt{2} - 1)$ . This can be done with methods such as linear programming [1] and basis pursuit [39].

Greedy reconstruction algorithm: Orthogonal Matching Pursuit (OMP) was one of the first algorithms explored to solve Eq. (10) which is simple and fast [24] to overcome the large running time of  $l_1$  since there is no known polynomial-time algorithm for linear programming [33] even its optimization is more efficient than the  $l_0$ . However, OMP has a major drawback because of its weaker guarantee of exact recovery than the  $l_1$  methods. To bypass these limitations, a modification to OMP called Regularized Orthogonal Matching Pursuit (ROMP) was proposed which recovers multiple coefficients in each iteration, thereby accelerating the algorithm and making it more robust to meeting the RIP [33]. In this technique, we use the ROMP algorithm for signal reconstruction

### 5.1.1 Super Resolution Ultrasound Compressed sensing

In our methodology, we utilize wavelets as our compression basis  $\Phi$  since they are good at representing images sparsely than non-localized bases for example Fourier. However, downsampling matrix  $\Theta$  in SR process involves point-sampled measurements, which lead to measurement matrix  $V$  that does not meet the RIP conditions due to incoherency. Intuitively, we can see that the better a basis is at representing confined features (such as wavelet), the more coherent it will be to point sampling because it can represent small spatial features (e.g., point samples) with only a less coefficients, by definition. Therefore, we propose to modify Eq. (14) depends on the observation that is filtering the high resolution image before downsampling. In other words, we can write our desired high-resolution image as  $x_r$  (the sharp version), which is then filtered by matrix  $\beta$  to result in a blurred, high resolution version  $x_b = \beta x_r$ . This blurred version is then downsampled by Eq. (13):

$$y = \Theta x_b = \Theta \beta x_r \quad (12)$$

In this approach, we choose a Gaussian filter  $\beta$ . Since it act as a multiplication by a Gaussian in the frequency domain we can define  $\beta = f^h G f$ , which makes Eq. (12):

$$y = \Theta f^h G f x_r \quad (13)$$

where  $f$  is the Fourier transform matrix,  $f^h$  is the inverse Fourier transform and  $G$  is a Gaussian matrix with values of the Gaussian function along its diagonal and zeros elsewhere. With this formulation in hand, we can now solve for  $x_r$  by posing it as a compressed sensing problem by assuming that its transform  $\hat{x}_r$  is sparse in the wavelet domain:

$$\min \|\hat{x}_r\|_0 \text{ s.t. } y = \Theta f^h G f \Phi \hat{x}_r \quad (14)$$

An approximate solution to this optimization problem can be achieved using greed methods. However, in order to solve  $q = Vx$ , where  $V^* = V^T$  with the assumption that  $\|V^TVA\| \approx \|A\|$  [33] greedy algorithms require having both the forward matrix  $V$  and backward matrix  $V^*$ . We have shown the forward Matrix  $V = \Theta\Phi\beta$ , where, the Gaussian matrix in  $\beta$  cannot be inverted through transpose, i.e.,  $G^{-1} \neq G^T$ , we use the backwards matrix of the form  $V^* = \Phi^T\beta^{-1}\Theta^T = \Phi^T f^h G^{-1} f \Theta^T$ .

We note that  $G^{-1}$  is also a diagonal matrix that is supposed to have the inversion of the Gaussian function of  $G$  along its diagonal. Whereas, we must be careful because of the well-known problem of noise amplification while inverting the Gaussian, we use a linear Weiner filter to invert the Gaussian function [35] to avoid noise, which means that our inverse matrix  $G^{-1}$  has diagonal elements of form  $G_{i,i}^{-1} = G_{i,i} / (G_{i,i}^2 + \gamma)$ .

The increases of the incoherence between the measurement and compression basis must be verified for proposed algorithm by computing the coherence with and without the blurring filter  $\beta$ .

The coherence can be found by taking the maximum inner product between any two basis elements scaled by  $\sqrt{n}$  [14]. When the Gaussian filter is introduced the coherence drops to 131.8. On the other hand, Without the Gaussian filter, the coherence is 243.6 for  $n = 380 \times 600$ . It's found that with Gaussian filter coherence reduction is enough to us apply the CS framework to this problem and get the high-quality results shown in the paper. With this formulation in place, we are now ready to solve the CS problem of Eq. (14).

In Eq. (14), we have shown the solution for the wavelet transform of the sharp, high-resolution image  $\hat{x}_r$ . We can take the inverse wavelet transform  $\Phi^* x_r$  once we solve for  $\hat{x}_r$ , to get the high-resolution image  $x_r$ . We use the ROMP greedy algorithm which is preferable over non-linear methods like linear programming [1] or basispursuit [3]. The algorithm is faster and can handle large vectors and matrices, which is vital when in images because the size of the matrices involved are  $n \times n$ .

The ROMP algorithm is similar to the OMP algorithm except the main difference is that instead of only selecting the largest coefficient, ROMP selects the continuous sub-group of coefficients with the largest energy, with the restriction that the largest coefficient in the group cannot be more than

twice as big as the smallest member. These coefficients are then added to a list of non-zero coefficients and a least-squares problem is then solved to find the best approximation for these non-zero coefficients. The approximation error is then computed based on the measured results and the algorithm iterates again. In this work, we limit the number of coefficients added in each iteration to obtain the better results.

#### 4.1.2 Experiments on Ultrasound Images

We applied the proposed method In vivo and phantom ultrasound images. The ultrasound images are obtained using COSMOS US diagnostic system. The parameters used to generate the phantom image: the lateral beam width was 1.5, the pulse width 1.2 and the center frequency was 5 MHz. The size of phantom image is 380 X 600 the images used in this experiments are shown in figures 1

The proposed CS approach for SISR is compared with Nonlinear-diffusion (ND) [37], Bicubic [38] and Yang et al. [39], to estimate the quality of reconstructed US images, the peak signal to noise ratio (PSNR) used. The PSNR defined by:

$$PSNR = 10 \log_{10} \frac{N_{\max}}{MSE} \quad (15)$$

where  $N_{\max}$ :The maximum fluctuations in the input image,  $N_{\max} = (2^n - 1)$ ,  $N_{\max} = 255$ , when the components of a pixel are encoded on 8 bits; MSE:denotes the mean square error, given by:

$$MSE = \frac{1}{MN} \sum_{i=1}^N \sum_{j=1}^M \left| O(i, j) - R(i, j) \right|^2 \quad (16)$$

where  $O(i, j)$ :the original image,  $R(i, j)$ :the restored image.

Figure 17 shows us the comparison of PSNR used different reconstruction Algorithm as we can see from the curve, compared with the ND, bicubic and Yang.et.al, the performance of proposed algorithm is better.

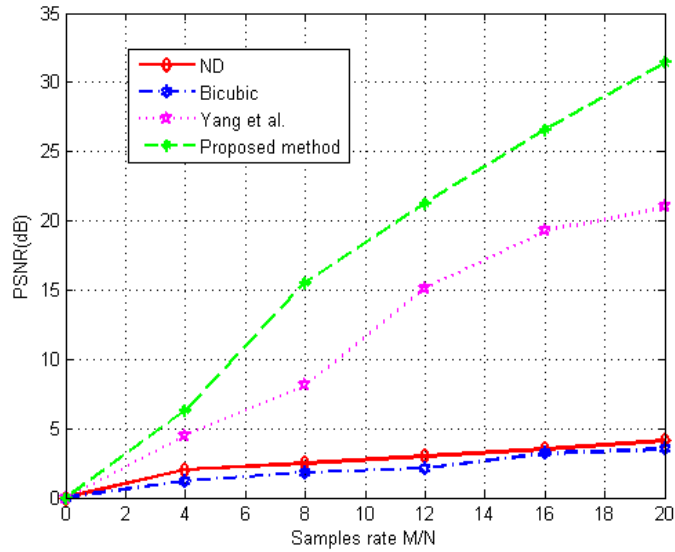


Figure 17: Comparison of PSNR for different reconstruction algorithm

Figure 18 represents recovered images by different methods. The amplification of the local regions of the recovery images is also shown in the right. From the result we can see that there are remarkable block effect in Non-diffusion method, Bicubic method and yang.et.al (shown in Fig. 18(a), (b) and (c)) recovers too smooth, distorted image and our proseed method can achieve better result than other

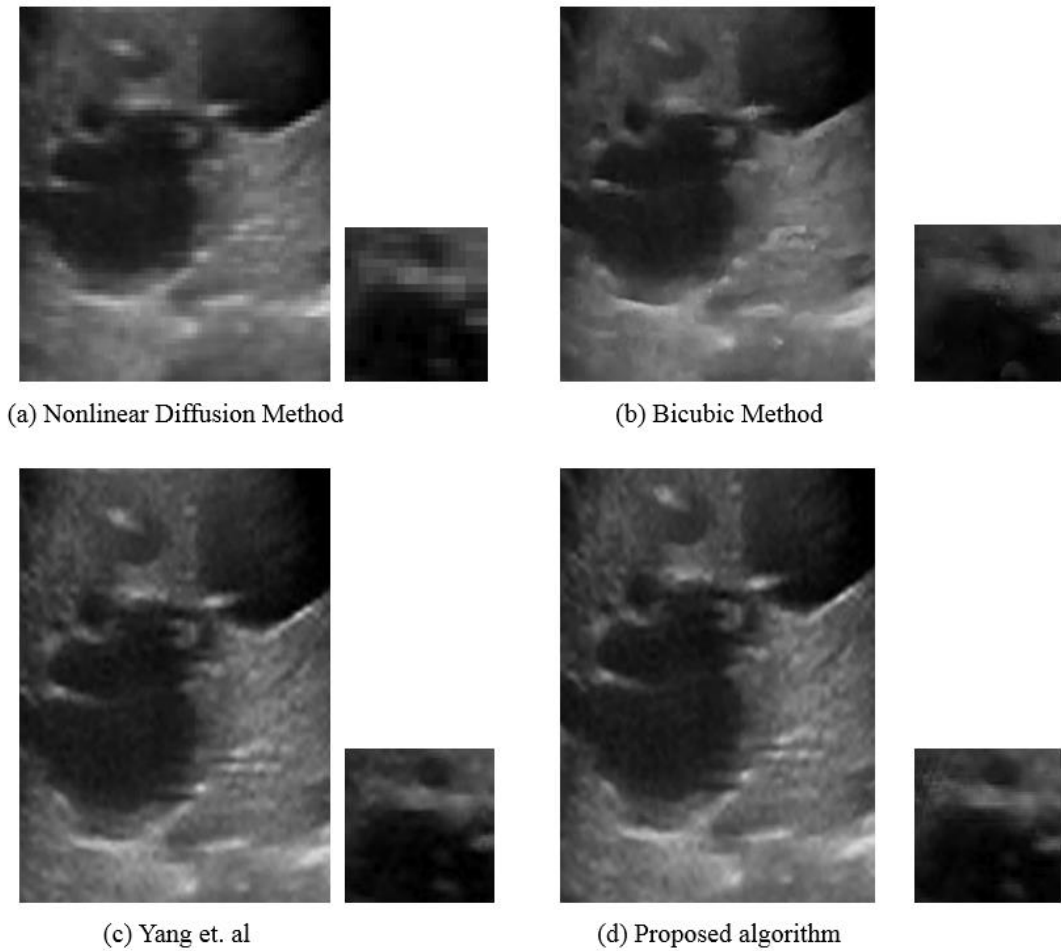


Figure 18(a-d): Reconstruction comparison of US images.

methods (shown in Fig. 18(d)) on detail preservation. To test our technique for clear visual comparison and accuracy by computing the root square error (RSE), a measure of the Euclidean distance, of their output to the original US high resolution image. In Figure 19 we plot RSE error variations for different magnifications level for various approaches and it is noted that our technique more information is available as the magnifications decreases so, the error reduced.



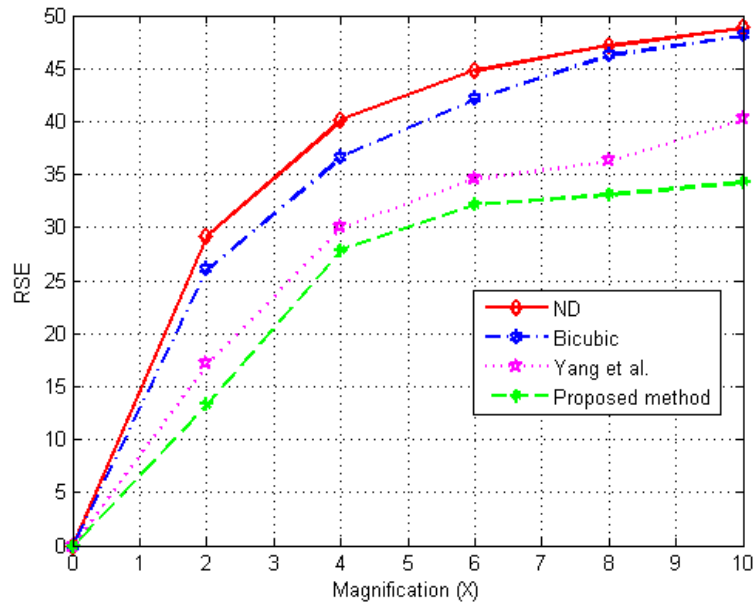


Figure 19: Reconstruction error comparison as a function of magnification level for the US phantom image.

The quantitative performance is measured with parameters like structural similarity (SSIM) [40] [41], mean structural similarity [42] and feature similarity (FSIM)[43] which compares the structure of two images by measuring the structural similarity, SSIM is related with the distortion of the visual sensing. The higher of SSIM and MSSIM are, much similar of the structure of the recovered image to the original image. Feature Similarity (FSIM) index is proposed based on the fact that human visual system (HVS) understands an image mainly according to its low level features [43]. It uses the phase congruency (PC) and gradient magnitude (GM) features of images as the evaluation index.

Table 3 shows the SSIM, MSSIM and FSIM of the reconstructed images obtained by different methods. From this we can see that the image recovered by our method is higher than that of the images obtained from the conventional methods mentioned in [37] [38] [39].

<b>Methods</b>	<b>FSIM</b>	<b>SSIM</b>	<b>MSSIM</b>
ND	0.7568	0.9543	0.6955
Bicubic	0.8231	0.9772	0.7593
Yang et al.	0.8467	0.9815	0.8067
Our Method	0.8538	0.9878	0.8114

Table 3: The numerical guidelines of the recovered images obtained from different methods.

### 4.1.3 Discussion and Conclusions

Our work is relevant to the techniques that attempt to solve the ill-posed problem of SR through regularization methods such as TV [44], [45]. However, the main difference between our approach and previous methods is that by posing it within the compressed sensing algorithm and tackle the problems by accessing tools like greedy Regularized Orthogonal Matching Pursuit (ROMP) algorithm we used in this paper.

We note that Yang et al. [24] also uses sparsity to regularize the problem of super-resolution whereas they uses dictionary of images and we use wavelet basis to sparsify the image. Neelamani et al. [46] proposed to combine wavelet and Fourier transforms together to reconstruct the signal, it's popularly known as, Fourier-Wavelet Regularized Deconvolution or ForWaRD. In our algorithm we use similar approach to reconstruct the image in the wavelet domain while same time inverse the signal in by using CS. This makes our algorithm to handle uncertainty due to down-sampling by assuming sparsity of the signal in the wavelet domain.

In this work, we have demonstrated the single image super resolution problem within the compressive sensing framework and utilize greedy matching pursuit algorithm to solve for the high resolution image. The uniqueness of our approach is based on the fact that we are not using the dictionary data for training. As a consequence, we could significantly recover images and reconstruct it in high resolution than conventional methods commonly used for these applications. Experimental results show that our method not only gives better performance but also an effective reconstruction on ultrasound images.

# Reference

- [1] E. Candès, J. Romberg, and T. Tao, “Robust uncertainty principles: Exact signal reconstruction from highly incomplete frequency information,” *Information Theory, IEEE Transactions on*, vol. 52, no. 2, pp. 489–509, 2006.
- [2] E. Candès and M. Wakin, “An introduction to compressive sampling,” *Signal Processing Magazine, IEEE*, vol. 25, no. 2, pp. 21–30, 2008.
- [3] D. Donoho, “Compressed sensing,” *Information Theory, IEEE Transactions on*, vol. 52, no. 4, pp. 1289–1306, 2006.
- [4] M. Lustig, D. Donoho, and J. Pauly, “Sparse MRI: The application of compressed sensing for rapid MRI imaging,” *Magnetic Resonance in Medicine*, vol. 58, no. 6, pp. 1182–1195, 2007.
- [5] F. Herrmann and G. Hennenfent, “Non-parametric seismic data recovery with Curvelet frames,” *Geophysical Journal International*, vol. 173, no. 1, pp. 233–248, 2008.
- [6] J. Jensen and P. Munk, “Computer phantoms for simulating ultrasound b-mode and cfm images,” *Acoustical Imaging*, vol. 23, no. 75-80, 1997.
- [7] J. Jensen, *Estimation of blood velocities using ultrasound: a signal processing approach*. Cambridge Univ Pr, 1996.
- [8] S. Goss, R. Johnston, and F. Dunn, “Comprehensive compilation of empirical ultrasonic properties of mammalian tissues,” *The Journal of the Acoustical Society of America*, vol. 64, p. 423, 1978.
- [9] S.A.Goss, “Compilation of empirical ultrasonic properties of mammalian tissues. ii,” *The Journal of the Acoustical Society of America*, vol. 68, p. 93, 1980.
- [10] M. Culjat, D. Goldenberg, P. Tewari, and R. Singh, “A review of tissue substitutes for ultrasound imaging,” *Ultrasound in medicine & biology*, vol. 36, no. 6, pp. 861–873, 2010.
- [11] P. Vandewalle, S. Susstrunck, M. Vetterli, Frequency domain approach to registration of aliased images with application to super resolution, *EURASIP Journal on applied signal processing 2006 (2006)* Article ID 71459.
- [12] C. Hendricks, L. Vliet, Improvement resolution to reduce aliasing in an under sampled image sequence, *In Proc. SPIE , Electronic Imaging 2000 Conference, San Jose 3965A (2000)* 214–222.
- [13] P. Vandewalle, M. Rumo, Super resolution in image using optical flow and irregular sampling.
- [14] R. Schultz, R. Stevansson, Extraction of high resolution frames from video sequences, *IEEE Transaction on image processing* 5 (6) (1996) 996–1011.

- [15] B. Tom, A. Akatsaggelos, N. Galatsanos, Reconstruction of a high resolution image from multiple degraded low resolution images, In Proc. IEEE Int. Conf. in Image processing, IEEE 3 (1994) 553–557.
- [16] S. Park, M. Park, M. Kang, Super resolution image reconstruction, IEEE Signal Processing Magazine 20 (3) (2003) 21–36.
- [17] H. Stark, P. Askoui, High resolution image recovery from image plane arrays, using convex projection, JOSA A (1989), 11, 1715-1726.
- [18] A. Tekalp, M. Zkan, M. Sezan, High resolution image reconstruction from lower resolution image sequences and space varying image registration, IEEE Int. Conf. acoustics, speech and signal processing, ICASSP, San Francisco, CA 3 (1992) 169–172.
- [19] “Nyquist-shannon sampling theorem.” Wikipedia, 2011. [http://en.wikipedia.org/wiki/Nyquist-Shannon\\_sampling\\_theorem](http://en.wikipedia.org/wiki/Nyquist-Shannon_sampling_theorem).
- [20] J. Tropp and A.C. Gilbert, “Signal recovery from partial information via orthogonal matching pursuit,” IEEE Trans. Inform. Theory, vol. 53, no. 12, pp. 4655-4666, 2007.
- [21] S.-J. Kim, K. Koh, M. Lustig, S. Boyd, and D. Gorinevsky. A method for large-scale  $l_1$ -regularized least-squares problems with applications in signal processing and statistics. Submitted for publication, 2007.
- [22] M. A. T. Figueiredo, R. D. Nowak, and S. J. Wright. Gradient projection for sparse reconstruction: Application to compressed sensing and other inverse problems. IEEE J. Selected Topics in Signal Processing: Special Issue on Convex Optimization Methods for Signal Processing, 1(4): 586–598, 2007.
- [23] I. Daubechies, M. Defrise, and C. De Mol. An iterative thresholding algorithm for linear inverse problems with a sparsity constraint. Comm. Pure Appl. Math., 57:1413-1457, 2004.
- [24] J. A. Tropp and A. C. Gilbert. Signal recovery from random measurements via orthogonal matching pursuit. IEEE Trans. Info. Theory, 53(12):4655–4666, 2007.
- [25] S. S. Chen, D. L. Donoho, and M. A. Saunders. Atomic decomposition by Basis Pursuit. SIAM J. 38 Sci. Compute. 20(1):33–61, 1999.
- [26] D. L. Donoho, Y. Tsaig, I. Drori, and J.-L. Starck. Sparse solution of underdetermined linear equations by stagewise Orthogonal Matching Pursuit (StOMP). Submitted for publication, 2007.
- [27] D. Needell and R. Vershynin. “Signal recovery from incomplete and inaccurate measurements via regularized orthogonal matching pursuit”. Submitted for publication, October 2007.
- [28] D. Needell and R. Vershynin. “Uniform uncertainty principle and signal recovery via regularized orthogonal matching pursuit”. Submitted for publication, July 2007.

- [29] S. G. Mallat and Z. Zhang. Matching pursuits with time-frequency dictionaries. *IEEE Trans. Signal Process.*, 41(12):3397–3415, 1993.
- [30] B. K. Natarajan. Sparse approximate solutions to linear systems. *SIAM J. Comput.*, 24:227–234, 1995.
- [31] E. J. Candès, “Compressive sampling,” in *Proceedings on the International Congress of Mathematicians*, 2006, pp. 1433–1452.
- [32] Y.P. E.J. Candes, A Probabilistic and RIPless Theory of Compressed Sensing, *IEEE Trans. Inf. Theory*. 57 (2011) 7235–7254.
- [33] D. Needell and R. Vershynin, “Uniform uncertainty principle and signal recovery via regularized orthogonal matching pursuit,” 2007.
- [34] E. J. Candès, “The restricted isometry property and its implications for compressed sensing,” *Comptes Rendus de l’Academie des Sciences, Paris, Serie I*, vol. 346, pp. 589–592, 2008.
- [35] R. C. Gonzalez and R. E. Woods, *Digital Image Processing*. Addison-Wesley Longman Publishing Co., Inc., 2001.
- [36] D. L. Donoho and X. Huo, “Uncertainty principles and ideal atomic decomposition,” *IEEE Trans. on Info. Theory*, vol. 47, no. 7, pp. 2845–2862, Nov 2001.
- [37] Wang, Bo, Cao Tian, Dai Yuguo, Liu Dong C”Ultrasound speckle reduction via super resolution and nonlinear diffusion”, In: ACCV, pp. 130–139.
- [38] R.G. Keys “Cubic convolution interpolation for digital image processing” *IEEE Transactions on Acoustics, Speech, & Signal Processing*, 29 (6) (1981), pp. 1153–1160.
- [39] J.C. Yang, J. Wright, T. Huang, Y. Ma”Image super-resolution via sparse representation”*IEEE Transactions on Image Processing*, 19 (11) (2010), pp. 2861–2873.
- [40] A.C. Brooks, X. Zhao, Structural similarity quality metrics in a coding context: exploring the space of realistic distortions, *IEEE Transactions on Image Processing* 17 (8) (2008) 1261–1273.
- [41] S.S. Channappayya, A.C. Bovik, Rate bounds on SSIM index of quantized images, *IEEE Transactions on Image Processing* 17 (9) (2008) 1624–1639.
- [42] Wang Z., Bovik A.C, Sheikh H.R, Simoncelli E.P.: Image quality assessment: from error visibility to structural similarity, *IEEE Transactions on Image Processing*, 2004, Vol 13(4),pp 600–612 .
- [43] L. Zhang, L. Zhang, X.Q. Mou, D. Zhang, FSIM: a feature similarity index for image quality assessment, *IEEE Transactions on Image Processing* 20 (2011) 2378–2386.
- [44] H. Aly and E. Dubois, “Image up-sampling using total-variation regularization with a new observation model,” *IEEE Transactions on Image Processing*, vol. 14, no. 10, pp. 1647–1659, Oct 2005.

- [45] S. Osher, A. Solé, and L. Vese, “Image decomposition and restoration using total variation minimization and the  $H^{-1}$  norm,” *SIAM J. of Multiscale Modeling and Simulation*, vol. 1, no. 3, pp. 349–370, 2003.
- [46] R. Neelamani, H. Choi, and R. Baraniuk, “Forward: Fourier-wavelet regularized deconvolution for ill-conditioned systems,” *IEEE Transactions on Signal Processing*, vol. 52, no. 2, pp. 418–433, Feb. 2004.